TECHNICAL REPORT BRL-TR-2946

BRL

1938 – Serving the Army for Fifty Years – 1988

IMPACT-GENERATED SURFACE AREA IN GUN PROPELLANTS

ROBERT J. LIEB

NOVEMBER 1988

U.S. ARMY LABORATORY COMMAND

BALLISTIC RESEARCH LABORATORY

ABERDEEN PROVING GROUND, MARYLAND

DESTRUCTION NOTICE

Destroy this report when it is no longer needed. DO NOT return it to the originator.

Additional copies of this report may be obtained from the National Technical Information Service, U.S. Department of Commerce, Springfield, VA 22161.

The findings of this report are not to be construed as an official Department of the Army position, unless so designated by other authorized documents.

The use of trade names or manufacturers' names in this report does not constitute indorsement of any commercial product.

UNCLASSIFIED
SECURITY CLASSIFICATION OF THIS PAGE

REPORT DOCUMENTATION PAGE

Form Approved OMB No. 0704-0188

1a. REPORT SECURITY CLASSIFICATION Unclassified	1b. RESTRICTIVE MARKINGS
2a. SECURITY CLASSIFICATION AUTHORITY	3. DISTRIBUTION/AVAILABILITY OF REPORT Unlimited
2b. DECLASSIFICATION/DOWNGRADING SCHEDULE	
4. PERFORMING ORGANIZATION REPORT NUMBER(S) BRL-TR-2946	5. MONITORING ORGANIZATION REPORT NUMBER(S)
6a. NAME OF PERFORMING ORGANIZATION US Army Ballistic Research Lab 6b. OFFICE SYMBOL (If applicable) SLCBR-IB-P	7a. NAME OF MONITORING ORGANIZATION
6c. ADDRESS (City, State, and ZIP Code) Aberdeen Proving Ground, MD 21005-5066	7b. ADDRESS (City, State, and ZIP Code)
8a. NAME OF FUNDING/SPONSORING ORGANIZATION 8b. OFFICE SYMBOL (If applicable)	9. PROCUREMENT INSTRUMENT IDENTIFICATION NUMBER
8c. ADDRESS (City, State, and ZIP Code)	10. SOURCE OF FUNDING NUMBERS PROGRAM ELEMENT NO. / PROJECT NO. / TASK NO. / WORK UNIT ACCESSION NO.
11. TITLE (Include Security Classification) IMPACT GENERATED SURFACE AREA IN GUN PROPELLANTS	
12. PERSONAL AUTHOR(S) Robert J. Lieb	
13a. TYPE OF REPORT TR 13b. TIME COVERED FROM ~~Jun 87~~ TO ~~Jun 88~~	14. DATE OF REPORT (Year, Month, Day) 15. PAGE COUNT
16. SUPPLEMENTARY NOTATION	

17. COSATI CODES		
FIELD	GROUP	SUB-GROUP

18. SUBJECT TERMS (Continue on reverse if necessary and identify by block number)
Gun Propellant, High Rate Testing, Mechanical Properties, IB Codes, Fracture Damage, Fracture Susceptibility

19. ABSTRACT (Continue on reverse if necessary and identify by block number)

The fracture damage suffered by gun propellant grains during the early part of the ballistic cycle greatly affects the evolution of chamber pressure and gun performance. Significant fracture can lead to the generation of pressure waves and catastrophic gun failure. It would be greatly advantageous if ballistic codes could provide predictions for the effect of grain fractures. To do this, the amount of fracture damage occurring due to the impact stresses must be known.

Much work has been done to characterize the mechanical response of propellant so that conditions under which embrittlement occurs are better understood. Fracture damage has been evaluated for impacted grains under a wide range of impact conditions and deviations from normal pressurization have resulted in calculated fracture generated surface area. However, these results are based on closed bomb pressure-time data. The calculations needed to generate the fracture surface area are laborious and are only reliable after a significant portion of the propellant has been consumed. In order to provide ballistic

20. DISTRIBUTION/AVAILABILITY OF ABSTRACT ☒ UNCLASSIFIED/UNLIMITED ☒ SAME AS RPT. ☐ DTIC USERS	21. ABSTRACT SECURITY CLASSIFICATION UNCLASSIFIED
22a. NAME OF RESPONSIBLE INDIVIDUAL ROBERT J. LIEB	22b. TELEPHONE (Include Area Code) (301)278-6195 22c. OFFICE SYMBOL SLCBR-IB-P

DD Form 1473, JUN 86 *Previous editions are obsolete.*

SECURITY CLASSIFICATION OF THIS PAGE
UNCLASSIFIED

BLOCK #19 (Continued)

codes with the information needed to predict the effects of grain fracture, a new and easily obtained relationship is needed. This report outlines the efforts to develop such a relationship, and the progress being made to incorporate fracture damage into ballistic codes.

TABLE OF CONTENTS

LIST OF ILLUSTRATIONS

I. INTRODUCTION

The role that propellant mechanical properties plays on gun performance during the interior ballistic cycle changes depending on the propellant response. If no propellant failure occurs during the ballistic cycle, the propellant mechanical response has no significant[1] effect on the resulting pressure. This is true because the pressurization rate within the gun depends only on the propellant surface area, and the burning rate. The surface area changes resulting from dimensional changes caused by increasing pressure are so small that, with no damage, the pressure profile is unaffected. However, when mechanical failure occurs resulting in an increase in the surface area available to the flame, significant deviations from the programed pressure profile can take place.

The magnitude of the undesired pressure increase depends on many interacting processes. The most significant of these is believed to be the total fracture generated surface area, the distribution of this newly created surface area within the propellant bed, and the time after ignition when grain failure does occur. To understand the failure mechanisms that result in high pressure malfunctions requires information that characterizes the propellant response under the high pressure dynamic conditions that are found within the gun during the early part of the interior ballistic cycle. High pressure gun failures due to propellant (not due to in-bore projectile detonations) usually happen before 5 percent of the in-bore projectile travel has occurred. Thus, the conditions which set up the breech overpressures occur very early in the cycle.

A breech blow scenario might proceed as in the following. Let us assume that the propellant is cold which tends to embrittle propellant. Also, assume that the igniter has been damaged so that a good distribution of igniter gasses is prevented and ignition is localized at the breech end. Either one of these conditions, by itself, may not be enough to cause excessive pressures to occur. However, in concert the overpressure possibilities are greatly enhanced. The ignition gases exert a force on the surface area presented by the grains starting a mechanical stress wave through the bed, and the interphase drag between the gas and solid surface as the gas flows through the bed accelerates the bed toward the forward end of the chamber. The low base pressure keeps the propellant in front of the stress wave in a mechanically weaker state, since it is known that dramatic increases in strength occur as pressure increases[2]. This results in propellant being subjected to mechanical shock and impact conditions that are likely to produce brittle failure. If the flame front follows this mechanical damage, large mass generation (in the form of gas) will result, which adds to the pressure gradient, and promotes further fracture and even more rapid burning. In this manner high amplitude pressure waves and excessive pressures are generated which can lead to gun failure.

Efforts have been under way for some time to characterize the mechanical response of gun propellant under conditions as close to operational as possible. It was recognized early that high strain rate response measurements would be required and that excursions into higher pressures would have to be made if proper propellant characterization was to be accomplished. The part that was not known, and to a large part still remains unknown, is the proper method required to relate the information that has been generated to the processes that control the pressure generation during this critical stage of combustion.

Apart from the performance, other questions with regard to system vulnerability may also be dependent on propellant mechanical response. Significant threats to system survivability arise due to the ignition of on-board propellant. This ignition threat occurs from two sources, behind the armor spall and shaped charge jet (SCJ) hypervelocity impact. It is apparent, again because of the fracture generated surface area, that propellant that has a brittle response to impact will provide a more violent response to the thermal spall threat. It is, therefore, important to maintain propellant integrity as much as possible to limit the response. The SCJ interaction with propellant is thought to be more complex. The direct initiation of the grains by the SCJ is probably not affected significantly by the propellant mechanical properties. However, in the regions surrounding this zone of direct initiation, the propagation of the detonation wave and the time needed to transition to deflagration may be heavily dependent on propellant mechanical response. Most of the mechanical response information presented here that applies to interior ballistic conditions, can also be applied to vulnerability threats with minor adaptations.

This paper will review the propellant fracture characterization progress made at the Ballistic Research Laboratory and show how this information is being applied to the problem of propellant mechanical failure.

II. TEST TECHNIQUES USED TO EVALUATE FRACTURE SUSCEPTIBILITY

The methods used to evaluate the fracture response were the Drop Weight Mechanical Properties Tester[3] (DWMPT), The Gas Gun Impact Tester[4] (GGIT), and the Mini-Closed Bomb[5,6] (MCB). These devices have been described in the the cited references, and only a brief description will be provided here.

The DWMPT provides a high strain rate (200 to 500/s) uniaxial compressive load to a single propellant grain specimen. Independent variables are temperature, impact energy, and a limited control of the strain rate regime. The output includes simultaneous measurement of engineering stress and strain, from which failure stress and strain along with other parameters can be determined, e.g. strain rate, modulus, toughness, etc. Over 2400 tests have been performed on gun propellants of all kinds. Measurements of Failure Stress, Failure Strain, Modulus, Strain Rate, Absorbed Energy Density (Toughness), have been successful and have demonstrated very acceptable standard deviations.

The GGIT provides impact damage to single unmodified propellant grains at a controlled velocity, temperature and impact orientation. It is a step closer to the type of conditions that grains are subjected during the ballistic cycle. The control is to within one degree Celsius for temperature, and to within 2 m/s for velocity. The grain damage is evaluated using the MCB so that the effects on combustion can be seen.

The MCB is a special, small volume, closed bomb that burns damaged grains. The rate of pressurization during combustion is controlled by the burning rate and surface area exposed to the flame. This enables the burning surface area to be determined once the burning rate of the propellant is known. When used in conjunction with the GGIT or DWMPT the surface area resulting from very

TABLE 1. M30 AND JA2 PERCENT PROPELLANT COMPOSITION

Component	JA2	M30
Nitrocellulose	59	28
NC Nitration Level	13.0	12.6
Nitroglycerin	15	22
Nitroguanidine	0	48
Ethyl Centralite	2	0
Diethylene Glycol Dinitrate	25	0
Akardit II	1	0

specific damage conditions can be determined. To obtain this fracture damaged surface area, the closed bomb pressure-time data usually used to determine propellant burning rate is inversely reduced to determine surface area.

As mentioned earlier, the details of the operation of these devices are contained in earlier reports. The limitation of the application of data to the problems of gun combustion will be discussed as appropriate in subsequent sections.

III. RESULTS OF PROPELLANT MECHANICAL PROPERTY TESTS

The discussion of fracture susceptibility will be focused on two types of tank gun propellant, M30, a triple base formulation, and JA2, a double base propellant of German formulation. The component formulations are found in Table I. These two propellants have been tested extensively in the DWMPT, GGIT, and the MCB. They have significantly different mechanical responses that affect the pressure generation very differently when fracture occurs. The mechanical response of M30 changes uniformly as a function of temperature. At high temperatures it fails in a plastic manner, but also fractures (tears or rips) as it fails. As the temperature is lowered, the amount of fracture increases and the response gradually becomes brittle. This progression is indicated by the response curves presented in Figure 1. Note that the stress at failure increases, and ability to maintain strength after failure decreases as the temperature is lowered. Figure 2 shows the Stress at Failure and the Modulus of M30 as a function of temperature over the range of ballistic interest. Similar curves are shown for JA2 in Figure 3. The JA2 is much softer, flows plastically, and shows no indication of fracture down to -20°C. At -40°C the plastic flow is shown to be dramatically reduced, although there is no indication of brittle failure in these curves. Figure 4 shows the Modulus and Stress at Failure curves for the JA2. The failure stress for this propellant is determined by the strain rate and temperature. JA2 does begin to fail in a brittle mode below -20°C, although the evenness of the stress distribution in the DWMPT does not cause fracture.

The curve in Figures 1 and 3 was created from five separate tests. The curves from each test condition were algebraically added together and then the resulting "sum" curve was divided by five. Figure 5 shows the results from a single M30 test at 18°C. The low scatter and preservation of curve details indicates the high degree of repeatability of these tests. However, there is some difficulty in

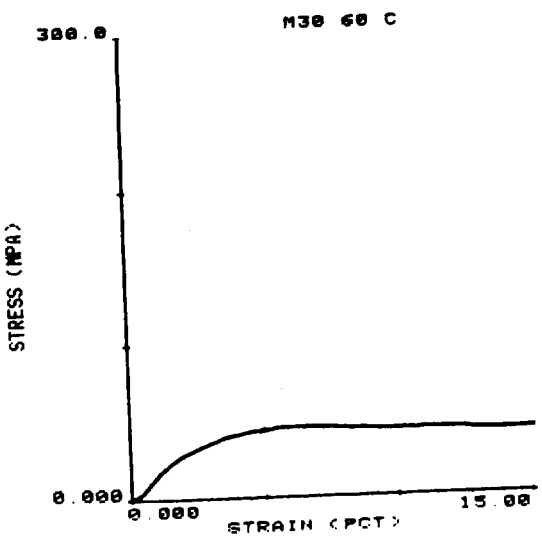

Figure 1a. 60°C

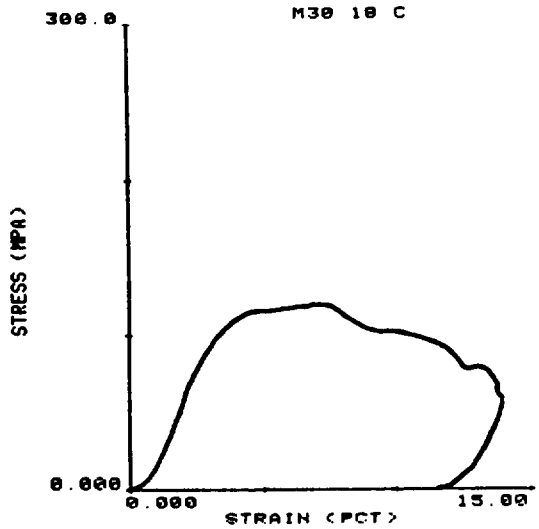

Figure 1b. 18°C

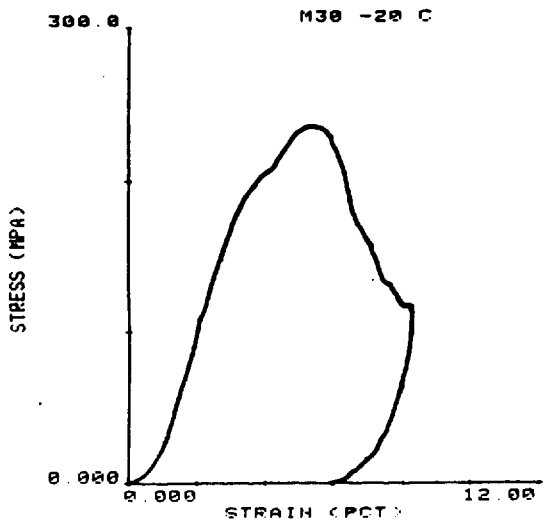

Figure 1c. -20°C

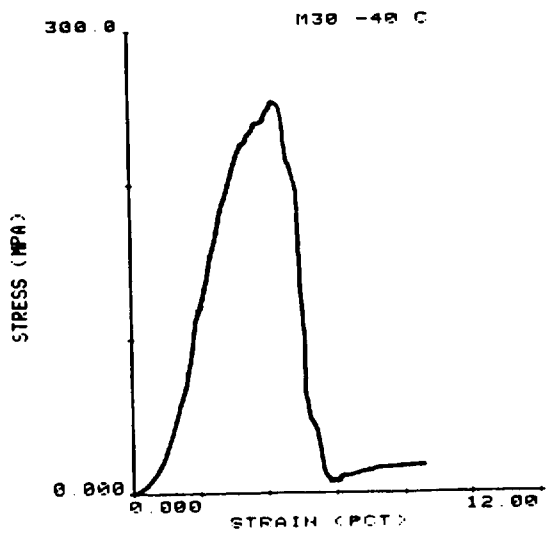

Figure 1d. -40°C

Figure 1. Stress vs Strain for M30 at a Strain Rate of About 250 s^{-1}

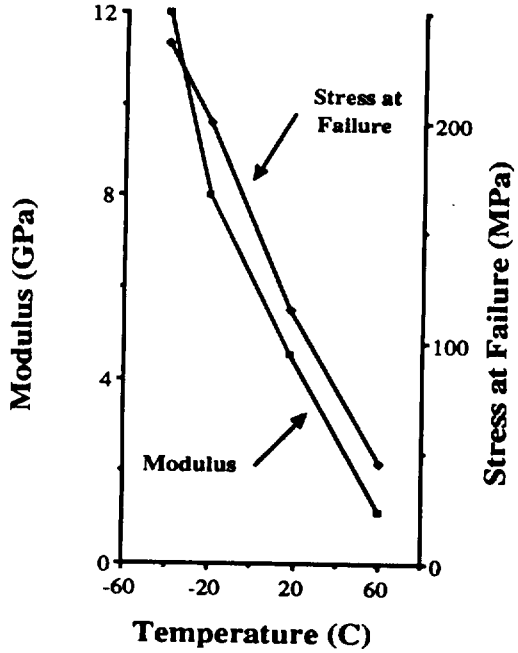

Figure 2. Modulus and Stress at Failure vs Temperature for M30 from DWMPT

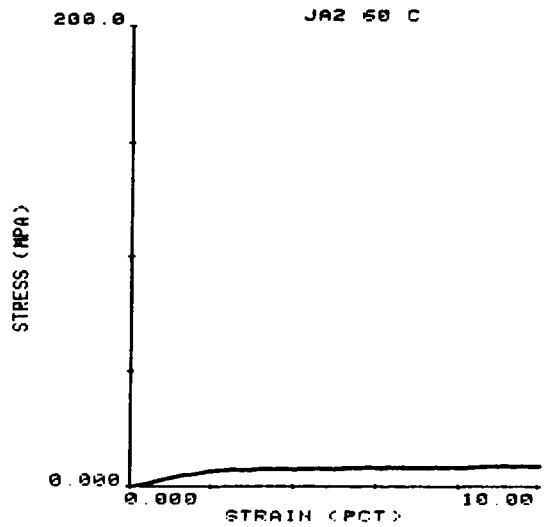

Figure 3a. 60°C

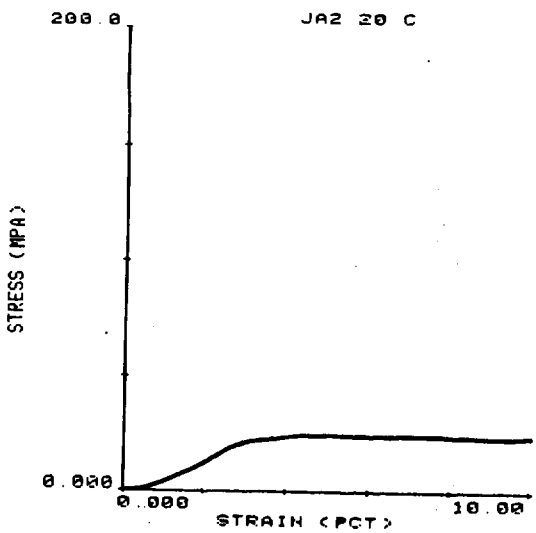

Figure 3b. 20°C

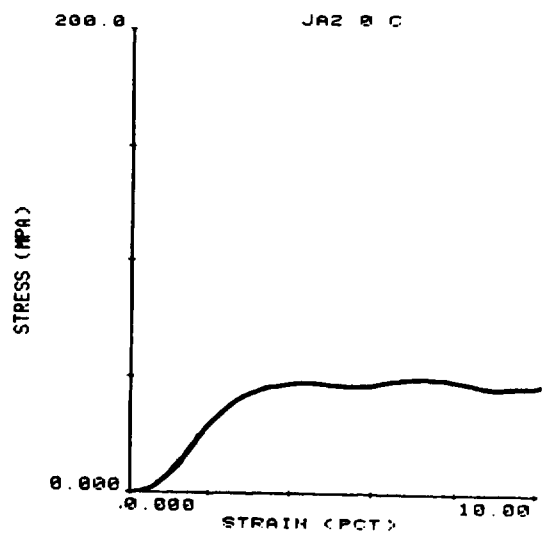

Figure 3c. 0°C

Figure 3. Stress vs Strain for JA2 at a Strain Rate of About 250 s^{-1}

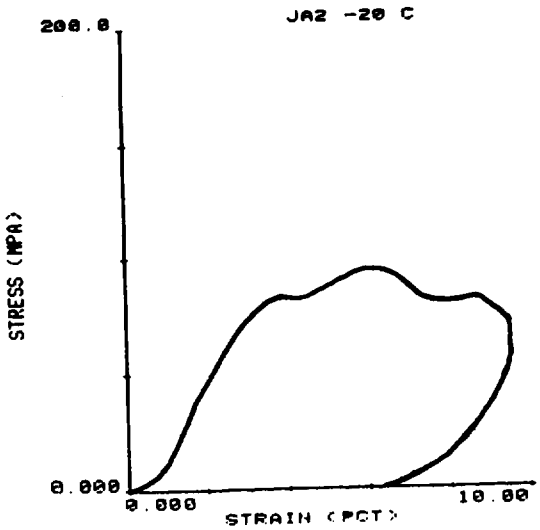

Figure 3d. -20°C

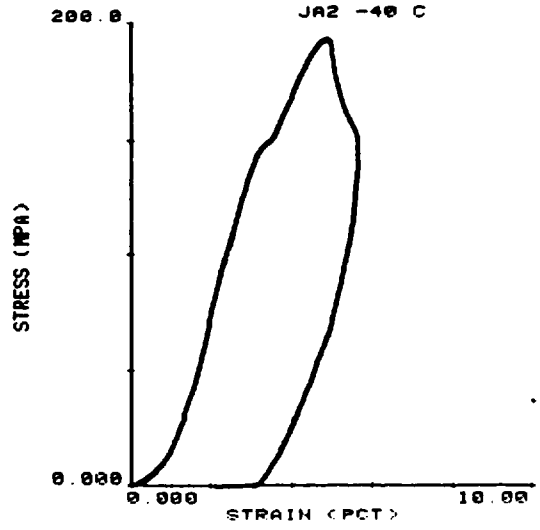

Figure 3e. -40°C

Figure 3. Stress vs Strain for JA2 at a Strain Rate of About 250 s^{-1}

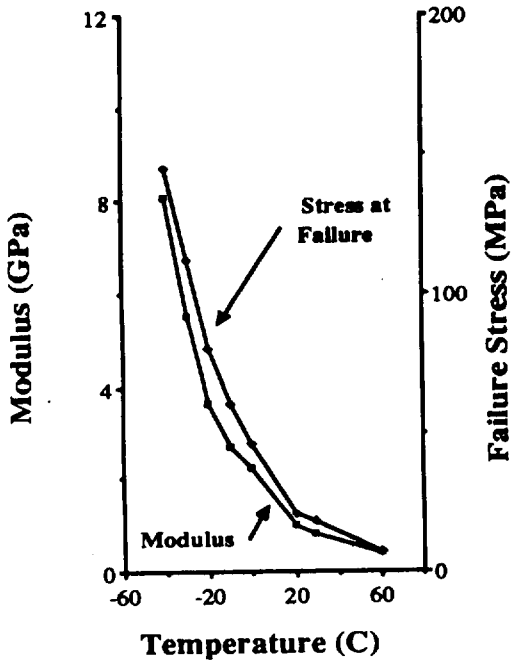

Figure 4. Modulus and Stress at Failure vs Temperature for JA2 from DWMPT

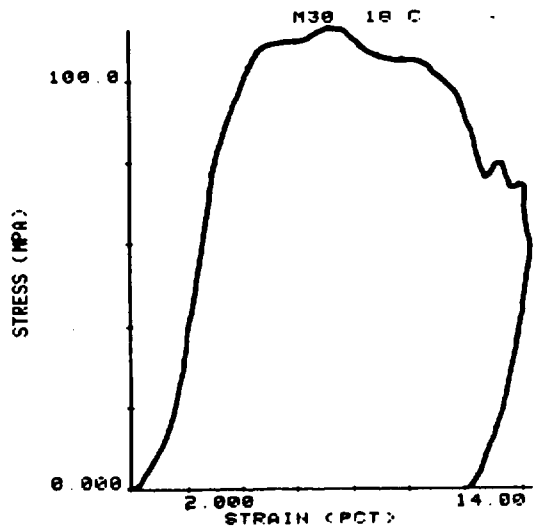

Figure 5. Data from a Single DWMPT Impact . Stress vs Strain for M30 at 18°C

extracting data from these curves as it relates to the fracture and combustion of propellant within the gun. The DWMPT information is generally used for characterization and relative strength assessment of propellants.

If a comparison is made among propellants of the same kind, where one variable (such as particle size or processing solvent concentration) is changed, then these curves can provide valuable information as to the stronger propellant, relative to the others. This type of information has been used many times to make decisions as to which process or particle size is most beneficial. However, if there are no comparison curves to gage the response, the prediction of fracture effects within the gun are unable to be made. This is partially the result of using engineering parameters that measure over regions before failure. As mentioned earlier, mechanical response has little effect on gun dynamics if no failure occurs. The process important in the gun is the mechanical response after failure takes place, and how that affects the pressurization.

IV. PROPELLANT FRACTURE EVALUATION

A. The Technique

With the above thoughts in mind, other approaches were taken to quantify the fracture response of propellants. The GGIT, which is a refined "shotgun" test[7], was developed to control the conditions under which grain fracture was induced. This test was soon coupled with the MCB which burned the damaged grains to determine how the damage affected the propellant burning. The results of many inverse reductions permitted the grain damage to be grouped into several categories, as shown in Figure 6. These curves represent actual data from several impact conditions. The Area Ratio axis represents the surface area available for combustion as a ratio to the original surface area of the grains. The Fraction Burned axis represents the fraction of the propellant charge that has been burned. The plots, then, show the evolution of available surface area as the propellant burns, which is important information for any fracture damage evaluation.

In Figure 6a, the theoretical or planned progression of surface area that is required for proper pressurization of the gun is shown for a seven-perforated grain. The increase in surface area as the grain burns is a feature that provides progressive burning and higher performance than normal degressive burning that occurs as most solid objects burn. This curve is provided in each surface area ratio plot as a point of reference. The manner in which the propellant actually burns is a measure of its performance and will be used in the fracture damage evaluation later. Each curve in Figure 6 is characteristic of the fracture condition of the grains as described below:

Figure 6a - (undamaged grains) As expected, there is a close match between the two curves for undamaged grains. Tested grains that show this type relationship can be said to have suffered no significant damage from the applied stress load.

Figure 6b - (DWMPT damaged JA2) If significant plastic deformation occurs during loading, the shape of the grain changes, which affects the surface area to volume ratio and lower than expected surface area results.

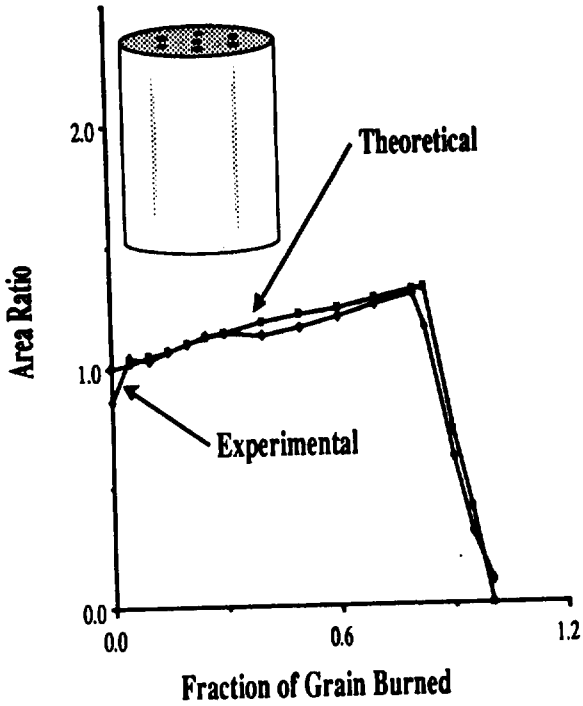

Figure 6a. Undamaged

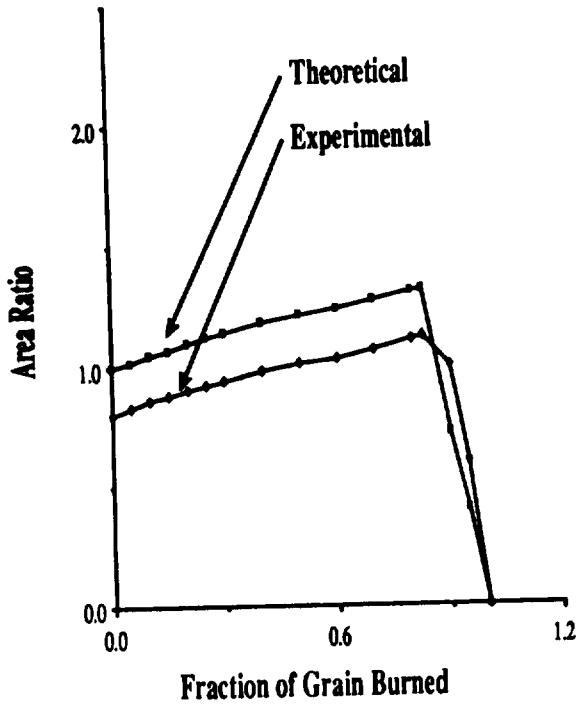

Figure 6b. Plastic

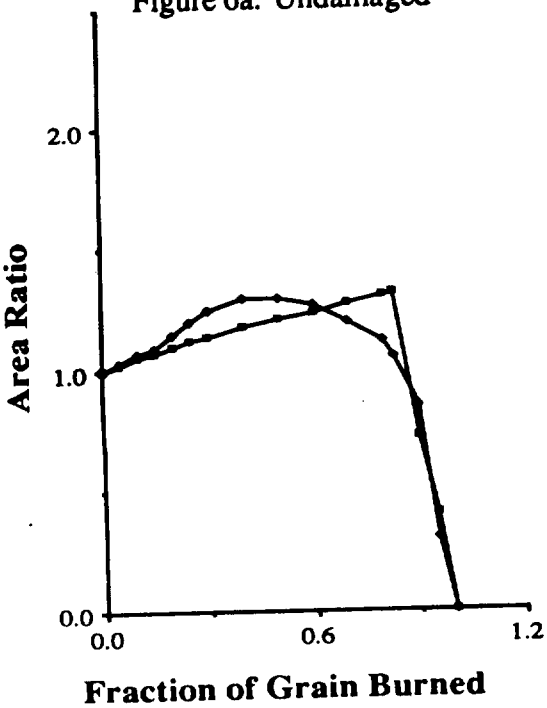

Figure 6c. Internal Fracture

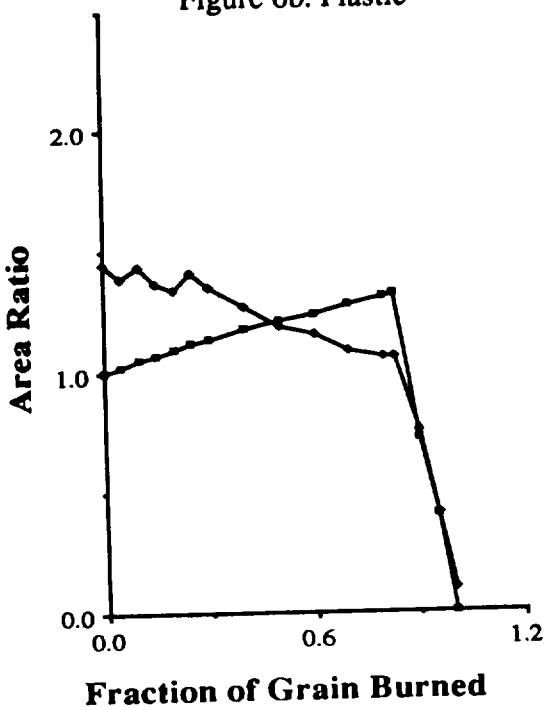

Figure 6d. Fracture into Large Pieces

Figure 6. Area Ratio vs Fraction Burned Profiles for Grains Damaged at Various Levels

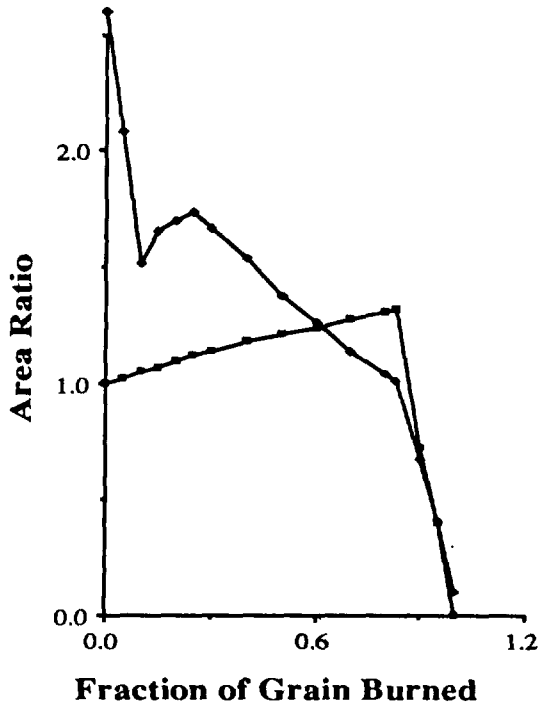

Figure 6e. BiModal Fracture

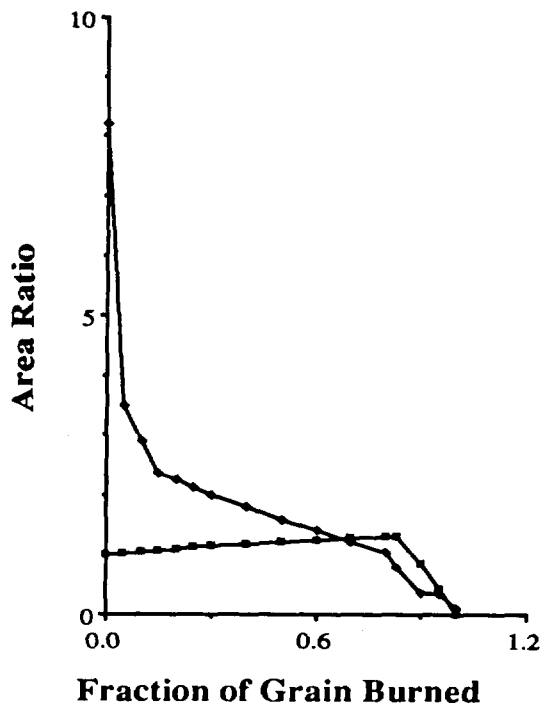

Figure 6f. Fracture into Small Pieces

Figure 6. Area Ratio vs Fraction Burned Profiles for Grains Damaged at Various Levels

Figure 6c - (GGIT damaged M30) A grain can show no visible damage after testing and still contain internal fracture or flaws which will lead to fracture during combustion. This curve results from such a situation, showing the fracture damage as it is uncovered.

Figure 6d - (GGIT damaged M30) When conditions become just severe enough for fracture to begin, large fragments are usually produced. The grain splits in half or into several large pieces. When this occurs, a curve similar to the one found here results.

Figure 6e - (GGIT damaged M30) If more severe conditions exist then found above, small shards or slivers can be produced. This results in a formation of a spike at low mass burned, as found here. The large surface area contained in the small mass of propellant rapidly burns off and the second peak emerges, produced by the remaining larger pieces which are still burning.

Figure 6f (GGIT damaged M30) - When impact conditions become so severe or the propellant is so brittle that many small pieces of about the same size are produced, this type of curve results. Finer fractured particles produce higher initial peaks and longer sustained burning at high surface area ratios.

As impact conditions become more favorable to fracture, the curve profile generally evolves from the "undamaged" to the "severe brittle fracture" representations. The rapidity with which the propellant profile goes through the various stages indicates the rate of increase in fracture

susceptibility for a given propellant. It should be noted here that no GGIT damaged propellant ever showed a curve similar to Figure 6b. When plastic flow occurs, it is usually associated with tearing or splitting which results in a overall increase in available area.

Fracture information in this form has significantly more value than in the form of mechanical properties information. As in the mechanical properties analysis, comparisons can also be made, so that an idea of the relative fracture susceptibility can be developed, but this information relates a specific damage condition to an increase in the surface area exposed to the flame. With this information a more applied evaluation of fracture effects can be made.

B. Results of M30 and JA2 Propellant Testing

The GGIT and MCB procedures described above were applied to seven-perforated M30 and JA2 propellant grains. Impact velocities ranged from 30 to nearly 120 m/s over a temperature range from 22 to -40°C. The data that shows the onset of grain damage is presented below.

M30 results are shown in Figure 7. Here the surface area ratio is plotted as a function of fraction burned, and each plot represents results over an impact velocity range of about 50 to 120 m/s at a particular temperature. Each particular curve is the result of about 10 grains that were impacted under the stated conditions, and burned in at least two MCB firings. In almost all the plots, the grains that were damaged under more severe conditions (higher velocities or lower temperatures) produced higher surface area ratios. The velocities are indicated in Figure 7c.

At 22°C damage begins to be indicated at the highest velocity. This curve shows that there was a high initial surface area that continued until about 50 percent of the grain was burned. A photo of a typical grain, Figure 8a, reveals the nature of the damage which can be described as splintering and tearing at the impact end of the grain. Damage at other velocities is minimal. At 10°C the propellant is not damaged at any velocity. It seems to be less fracture susceptible than at the higher temperature. A more accurate statement may be that it tears less easily. At 0°C large fragments, Figure 8b, result at 85 m/s, and at 105 m/s significant amounts of small fragments, Figure 8c, begin to be formed. At -10°C M30 shows fracture damage at all velocities and increasing damage as velocity increases. At -20°C there is still a distribution of damage, but the higher velocity fracture begins to produce curves that look similar except for the amount of very small particles produced, see Figure 8d. At -30 and -40°C the damage is very similar at all velocities. The higher velocity impacts tend to result in higher initial values of surface area and continued higher values as burning progresses. The continuance of high surface area levels into large fraction burned values plays a significant role in the production of rapid high pressure generation within the gun.

Figure 9 shows the same information as found in Figure 7, but here each plot represents results over a temperature range of 22 to -40°C at a particular velocity grouping. These curves show that, except for the decrease in surface area at 10°C, surface area generation increases uniformly as temperature is reduced.

Similar information is presented for JA2 in Figure 10. No significant fracture damage was indicated at any velocity above -10°C, as shown in Figure 10a. At -20°C fracture occurs at all

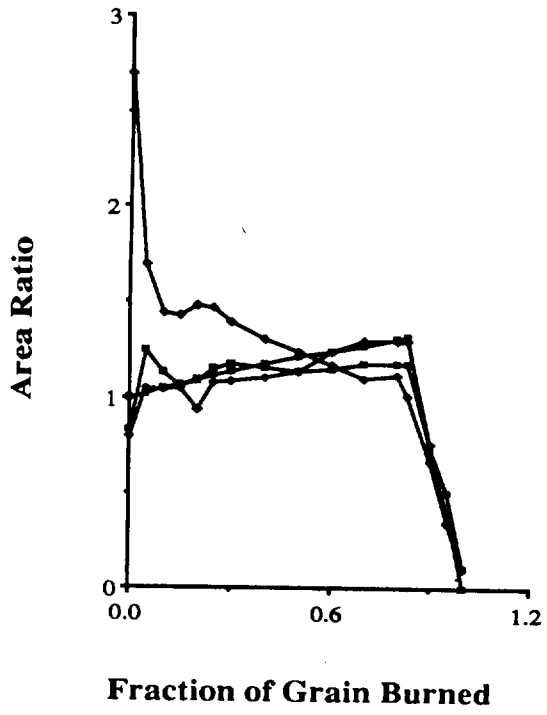

Figure 7a. 22°C

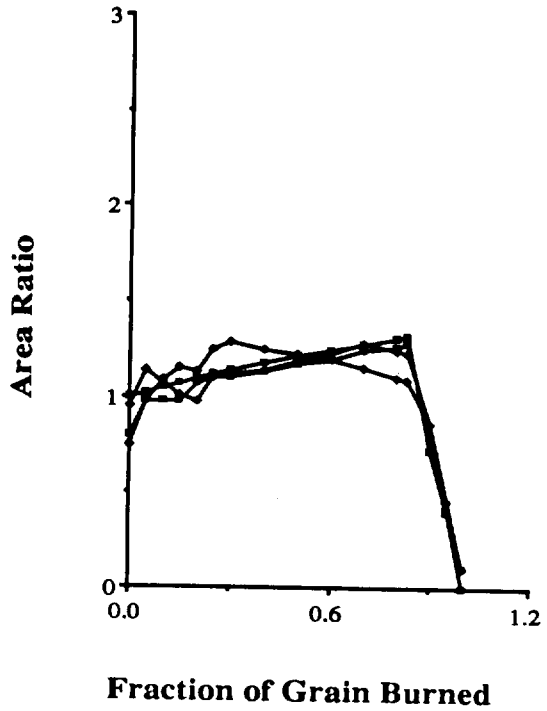

Figure 7b. 10°C

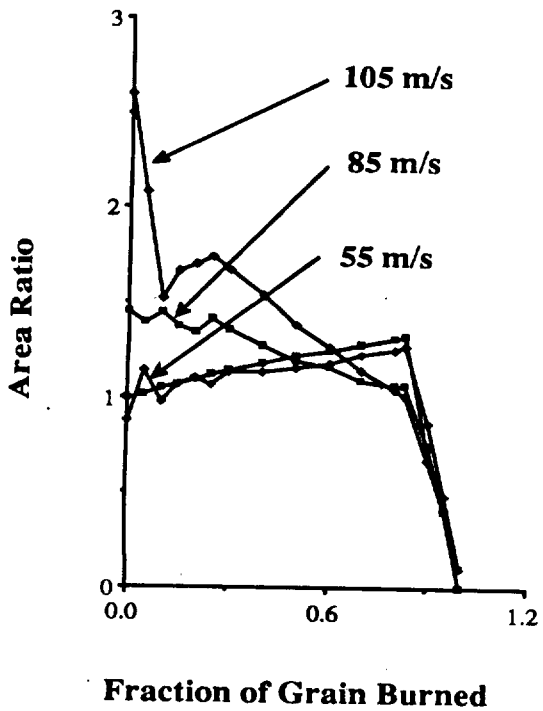

Figure 7c. 0°C

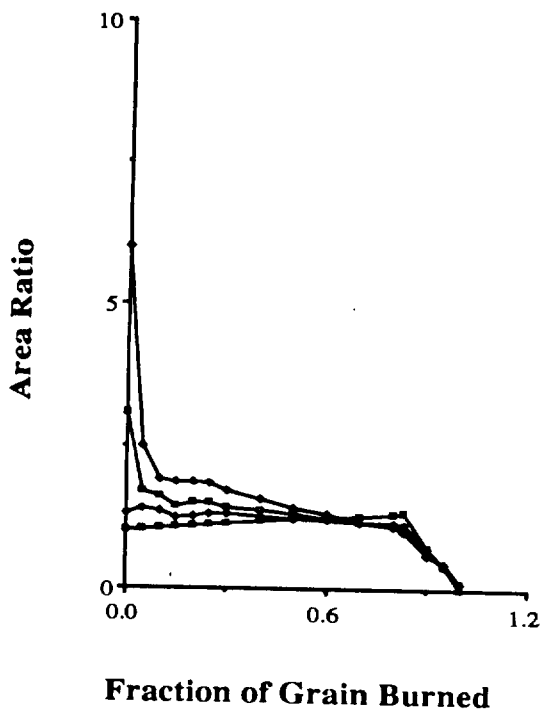

Figure 7d. -10°C

Figure 7. Area Ratio vs Fraction Burned for GGIT Damaged M30 Propellant Grains

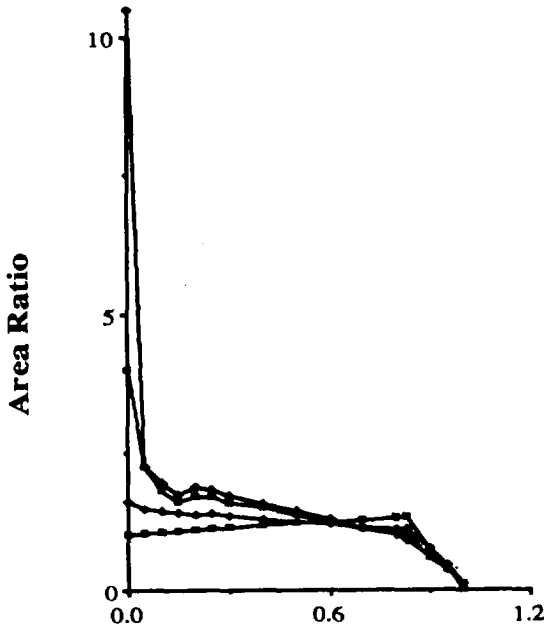

Figure 7e. -20°C

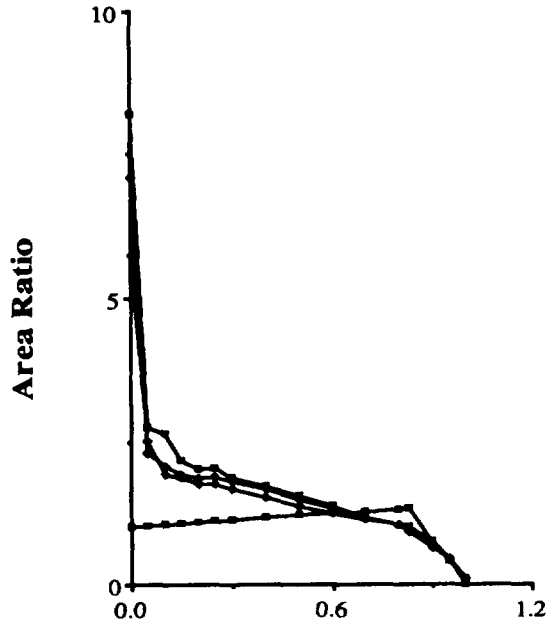

Figure 7f. -30°C

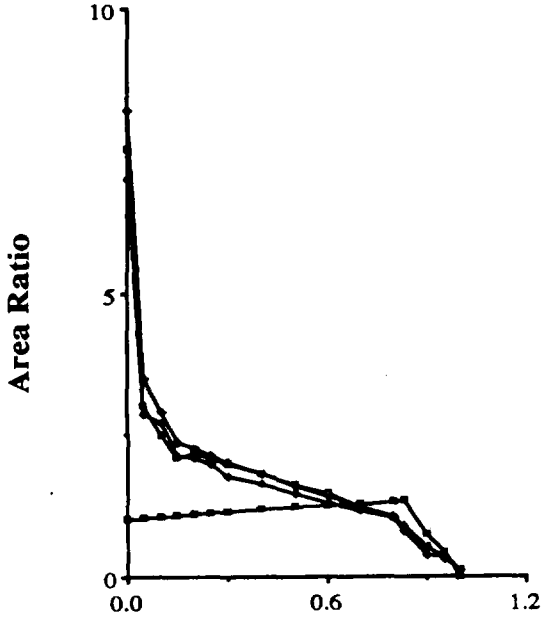

Figure 7g. -40°C

Figure 7. Area Ratio vs Fraction Burned for GGIT Damaged M30 Propellant Grains

velocities and is significant at impact velocities of 115 and 90 m/s. At these speeds small shards as well as large fragments are produced, as found in the photograph in Figure 11a. This indicates a sudden onset of brittle response. At -30 and -40°C the amount of fracture increases dramatically. The extension of large surface area into 60 percent fraction burned seems specially significant. As for the M30, as conditions become more favorable for brittle fracture, the initial and extended surface area increase. Figure 11b shows a photograph of fracture damage at 115 m/s and -30°C.

Figure 12 shows the same information as presented in Figure 10, but in the Figure 9 format. In each plot, the onset of fracture begins at -20°C and worsens as the temperature is reduced.

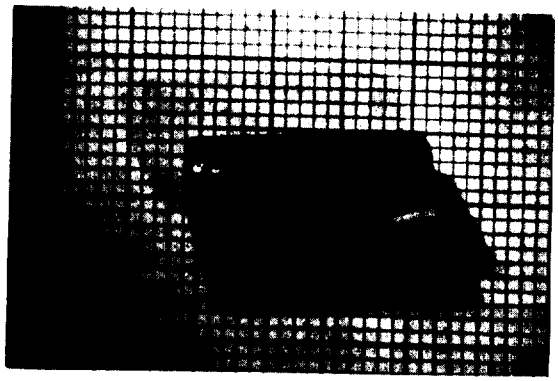

Figure 8a. 22°C at 115 m/s

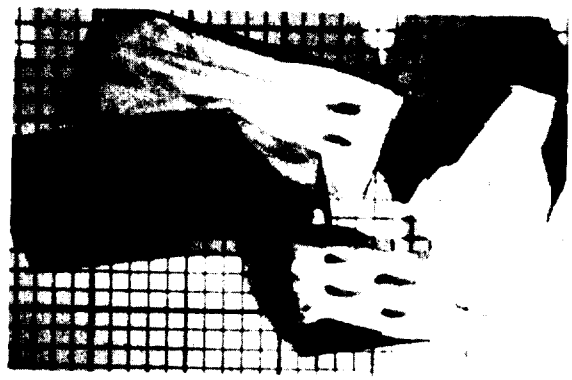

Figure 8b. 0°C at 85 m/s

Figure 8c. 0°C at 105 m/s

Figure 8d. -20°C at 105 m/s

Figure 8. Photographs of GGIT damaged M30

V. DATA INTERPRETATION

A. DWMPT Data

A quantity, called the Absorbed Impact Energy Density, was considered as a fracture susceptibility parameter from DWMPT results, and was based on a toughness-type calculation. Toughness is usually a measure of how much energy per unit volume (megajoules per cubic meter or MPa) a material can store or otherwise absorb before some failure limit is reached. A material that can withstand a higher stress or a greater strain before failure has the ability to absorb greater energy before failure than one that cannot. If this concept is applied to propellants several things enter that cause complication. As mentioned earlier, mechanical response before propellant failure does not influence ballistic performance. This means that the domain over which the toughness calculation is made needs to be modified to include the post-failure response. Also, propellant material is not a linear elastic structural material. It is more of a viscoelastic, viscoplastic, nonlinear composite. Because of this, the mechanical response depends to a large extent on the method of load application. This results in a more complex response than expected from structural materials, and obscuring the usual meaning associated with toughness when applied to these materials.

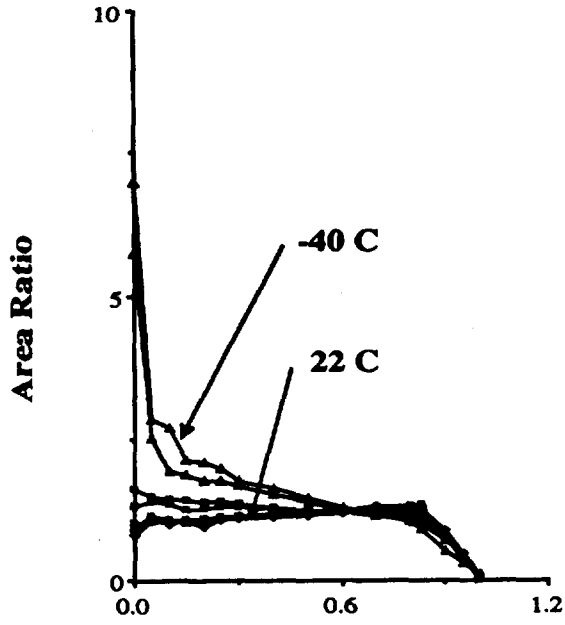

Figure 9a. About 60 m/s

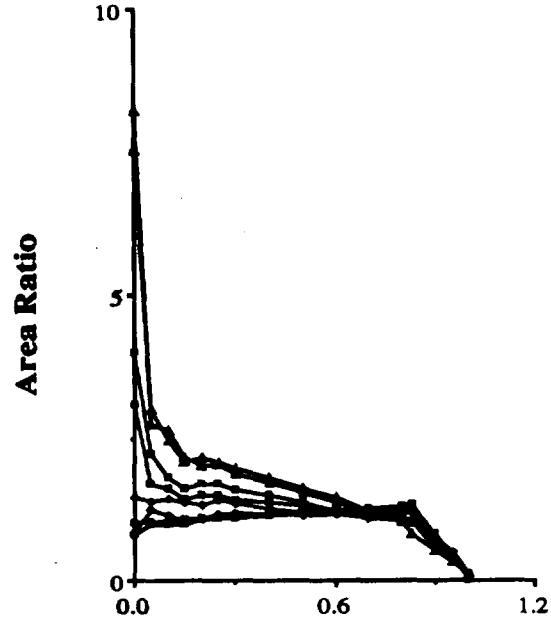

Figure 9b. About 90 m/s

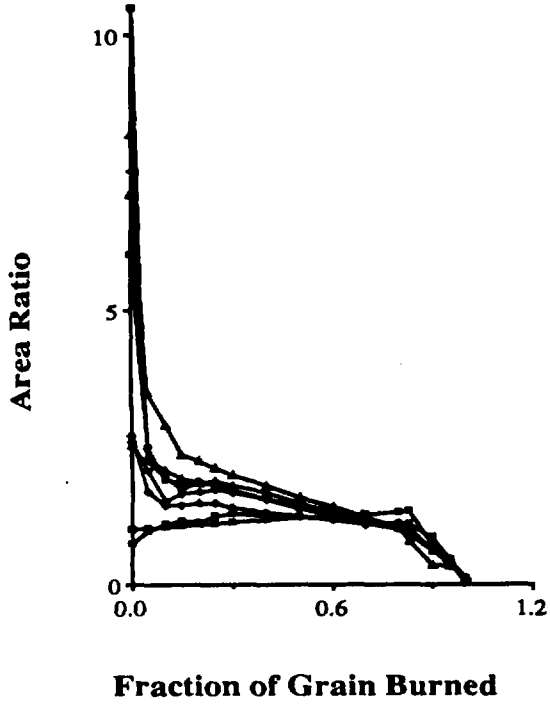

Figure 9c. About 105 m/s

Figure 9. Area Ratio vs Fraction Burned for GGIT Damaged M30 Grouped by Velocity

Toughness calculations have been made on each specimen subjected to DWMPT. The parameter, τ, is calculated by integrating the stress over the strain for the entire impact event, as shown in Figure 13a. The value of the integral is defined as the absorbed impact energy density, and it describes the net amount of work per unit volume that was performed on the propellant specimen during impact. If the grain were perfectly elastic, this value would be 0. The amount of energy supplied to the grain would be returned to the system during the unloading process. If the grain were perfectly plastic the value would be the flow stress multiplied by the total strain. Results are usually presented as a percentage of the maximum energy density (potential energy of the drop weights divided by the initial volume of the specimen). Unless the propellant suffers very severe brittle fracture, values of about 0.8 are obtained for nearly all propellants. This seems to be independent of the initial energy available but does show a

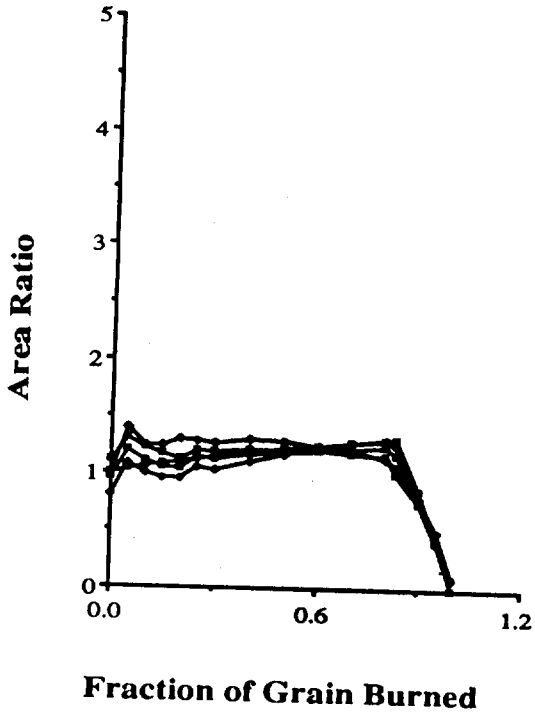

Figure 10a. -10°C

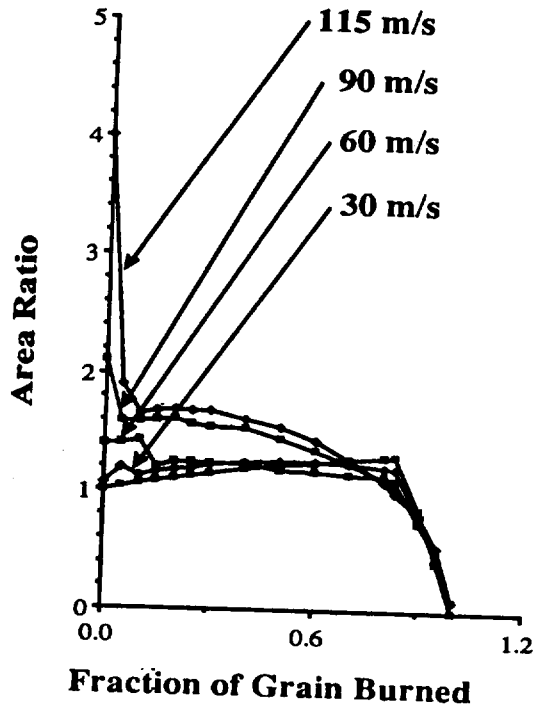

Figure 10b. -20°C

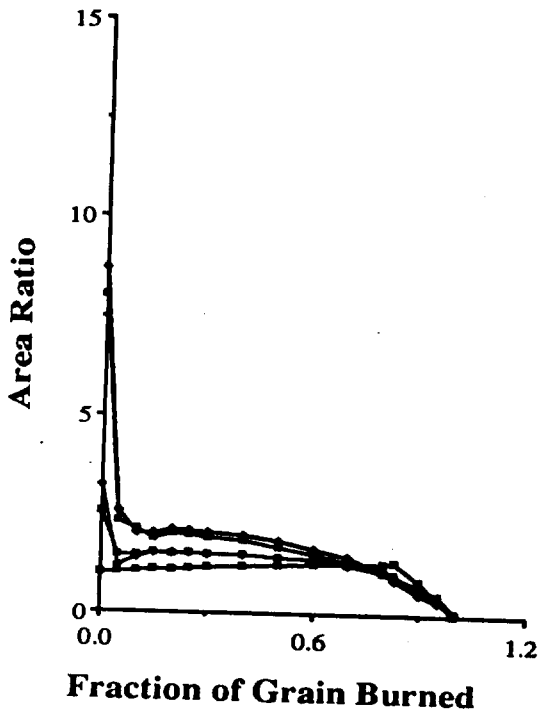

Figure 10c. -30°C

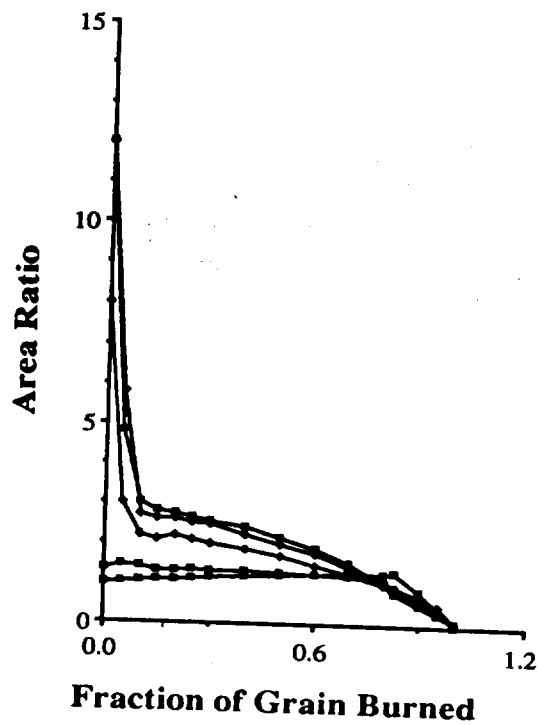

Figure 10d. -40°C

Figure 10. Area Ratio vs Fraction Burned for GGIT Damaged JA2 Propellant Grains

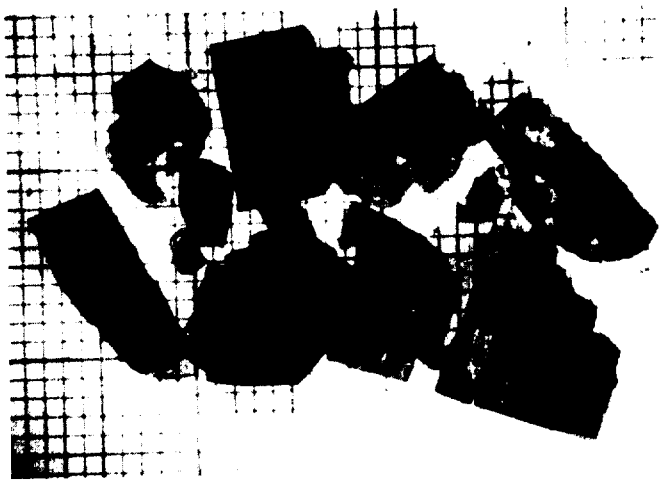

Figure 11a. -20°C at 90 m/s

Figure 11b. -30°C at 115 m/s

Figure 11. Photographs of GGIT Damaged JA2 Grains

dependence on strain rate. The ratio tends to go down for higher rates. This could mean that the grains are becoming more elastic and returning more energy to the system, or it could mean that the grains are becoming more brittle and are unable to absorb as much impact energy. Figure 13b shows how little this parameter varies for M30 over the temperature range that the propellant goes from plastic to very brittle behavior. Attempts to separate the categories into which the energy is flowing during

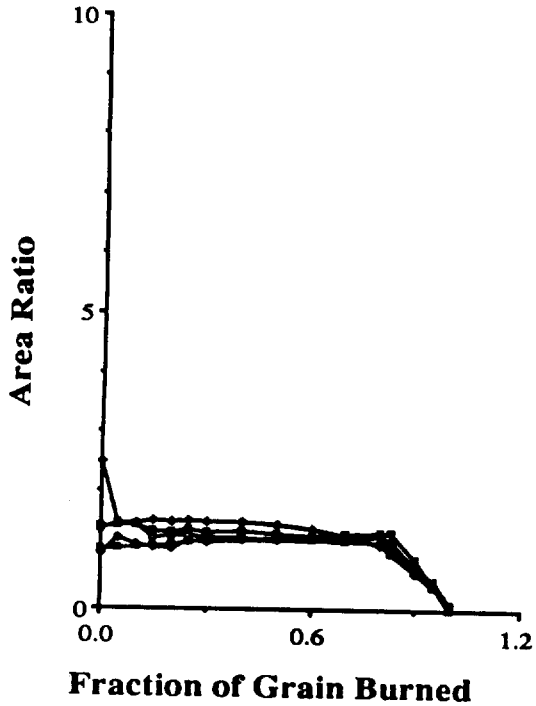

Figure 12a. About 30 m/s

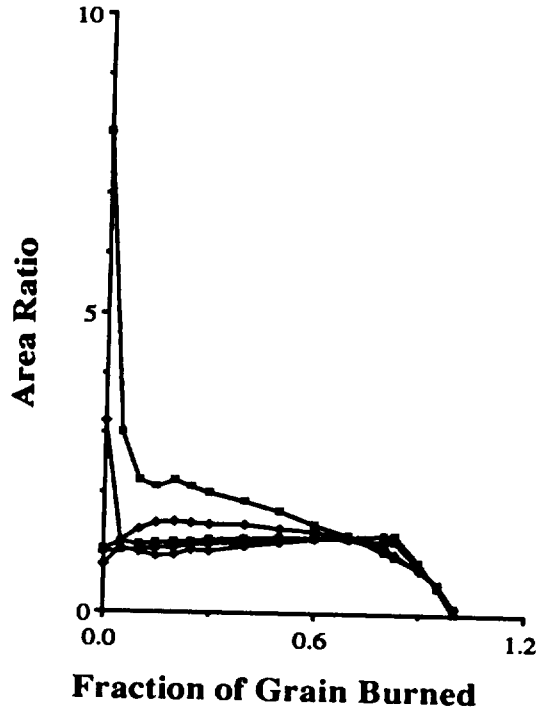

Figure 12b. About 60 m/s

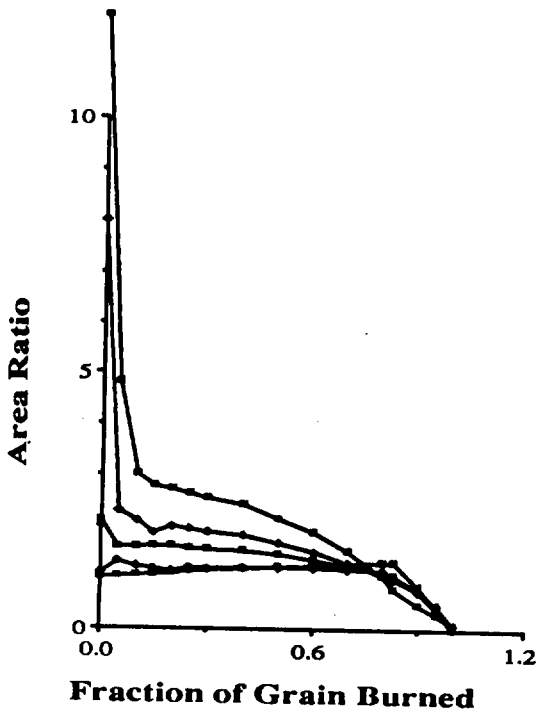

Figure 12c. About 90 m/s

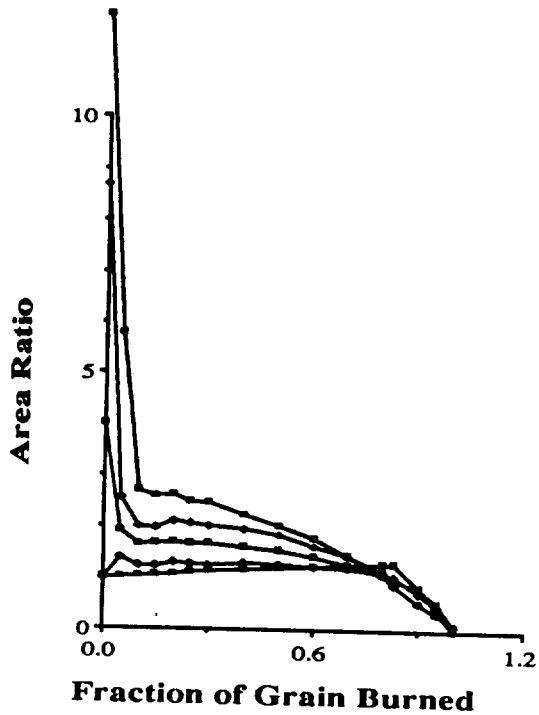

Figure 12d. About 115 m/s

Figure 12. Area Ratio vs Fraction Burned for GGIT Damaged JA2 Grouped by Velocity

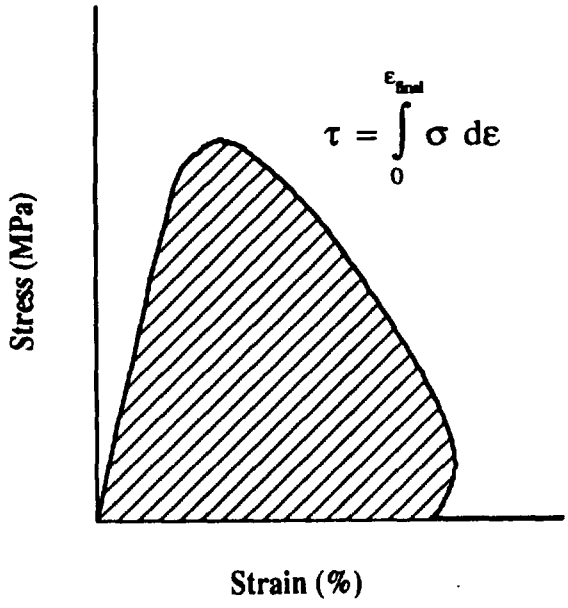

Figure 13a. Schematic Diagram Indicating the Value of τ

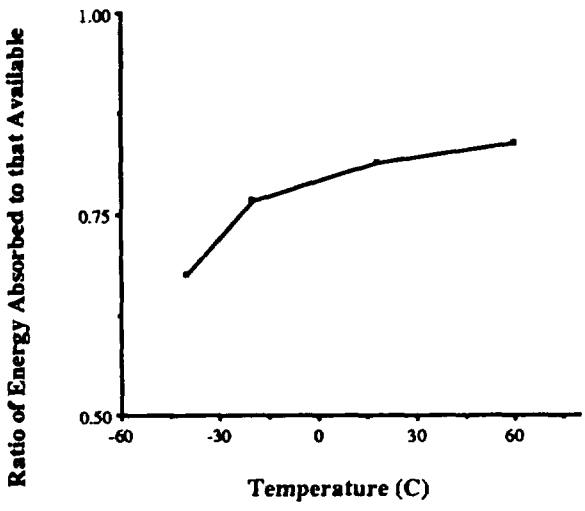

Figure 13b. Ratio of τ to Maximum Impact Energy Density Available vs Temperature for M30

Figure 13. The Absorbed Impact Energy Density Parameter

impact have been frustrated by the propellant response changing when conditions are altered to isolate the variables. It is hoped that when the high rate servohydraulic test facility is brought on line, which will permit much greater control over the rate and energy of impact, these questions will be able to be more clearly addressed.

B. GGIT and MCB Data

Attempts were also made with some success to further quantify the fracture generated surface area results. It was felt that poor performance would be indicated by how far the actual surface area profile deviated from the programed or theoretical curve. A parameter, called the Total Deviation (TD), was defined to measure the magnitude of this deviation. It was calculated according to the following method. The absolute difference between the actual Surface Area Ratio vs Fraction Burned and the theoretical profile was calculated. The resulting curve represented the deviation from programed burning brought about by propellant damage. The curve was then integrated over the entire fraction burned, and that value was assigned as the TD for that propellant under the associated fracture conditions.

The advantages of the TD value were several. The parameter was intrinsic in nature, so that different granulations and formulations could be compared. The parameter was based on the deviations in propellant burning caused by mechanical damage, so that its value related these two phenomena. It was easy to calculate once the surface area information was available. It could be used as a vehicle to obtain critical parameters (critical impact velocities or critical temperatures[6]) that related directly to interior ballistic conditions. Finally, changes in TD reflected conditions under which the fracture susceptibility was undergoing significant change.

There are two major disadvantages of TD. First, it uses the surface area ratio deviation over the entire fraction burned for its calculated value when only a fraction of the propellant is burned before overpressure occurs (overpressure is about 1 GPa). Second, it is a parameter of arbitrary value that is not easy to use by itself or in conjunction with other gun parameters to directly predict gun propellant behavior. Figure 14a shows the result of TD calculations for JA2 taken from Reference 6. In this report the parameter was able to establish a fracture susceptibility difference between two chemically identical JA2 formulations that were produced at two different sites that used different processing procedures.

C. Summary

To summarize the procedure as it now exists, propellant fracture susceptibility is evaluated by a combination of the above two processes. The easiest procedure is DWMPT evaluation. Here intrinsic high rate mechanical properties of the propellant can be determined over the temperature range of ballistic interest. Comparisons can be made between properties of known or similar propellants and evaluated on that basis. These tests provide information as to how changes that are being considered to improve performance have to be balanced against any resulting deleterious changes in mechanical response. These tests also provide insight into the role that mechanical properties may play in deviant ballistic pressure phenomena. Secondly, the relationship between mechanical response and how that mechanical response affects propellant combustion has been bridged by the controlled impact damage of the DWMPT and the GGIT, and the surface area analysis capability offered through the MCB and the corresponding closed bomb analysis. The generation of this information is significantly more labor intensive than the DWMPT procedure, but it is also unique, as explained earlier. The information in this form can be used to establish parameters that relate directly to gun conditions (critical velocity) and can be used to estimate the fracture generated surface area due to impact in interior ballistic codes, explained below.

VI. NEW METHODS FOR EVALUATING FRACTURE SUSCEPTIBILITY

A. The Need for a New Parameter

The establishment of a parameter that would characterize the the fracture susceptibility of gun propellants would greatly aid the evaluation of new and existing propellants. Ideally the measurement of this parameter would be relatively simple and would indicate how much fracture generated surface area would be made available from grains damaged under specific temperature, pressure and loading rate conditions. To probe the nature of what must be included in such a parameter, some points about what is recognized as being important should be explained.

The most important single factor influencing the pressurization rate of a particular propellant is the surface area. The pressurization rate is directly proportional to the mass generation rate which can be expressed by the following relationship:

$$\frac{dm}{dt} = A \rho \frac{dr}{dt} \quad , \qquad (1)$$

where m is the mass of gas present, t is time, A is the instantaneous surface area of the propellant, ρ is the mass density, and dr/dt is the linear burning rate of the propellant. The burning rate is a function of pressure that usually follows the following form:

$$\frac{dr}{dt} = a + b P^n , \qquad (2)$$

where a, b and n are constants, and P is the instantaneous pressure. The pressure is directly related to the mass of propellant burned. Therefore, the rate of pressurization at any time depends only on the surface area and the pressure. However, how that surface area evolves as the propellant burns is equally important.

As an example, consider the following. It is possible that fracture damaged propellant from two different fracture conditions could produce the same initial fracture damage surface area. Assume that this surface area ratio is 4 in both cases. If in the first case the mass associated with the fracture damaged area is a very small amount, then dm/dt will be very high for a very short while, and will then fall to near normal values without much of a pressure deviation. If, in the second case, the mass associated with the fracture damaged area is distributed over a significant portion of the total charge, then dm/dt will be very high initially, and will remain high for an extended duration. The high rate mass generation will be further aggravated by the higher pressures as they are generated. What this means is that while the initial surface area for M30, GGIT damaged at 105m/s and -20°C, is much higher than for those grains damaged at the same velocity at -40°C (Figure 9c), the greater surface area at higher fraction burned found in the -40°C case will produce a greater pressure deviation.

B. Modification of the Total Deviation

Many attempts have been made to incorporate the above observation into a parameter. The TD parameter, which has been used to evaluate the deviation as described earlier, accounts for the magnitude of deviation, but over the entire burn, rather than selecting or weighting the deviation where it most influences the mass generation. Attempts to weight this distribution properly have involved using the TD approach only up to specific value of fraction burned. This, however, does not account for the more rapid combustion that fractured grains undergo. An example of a recent analysis that does attempt this consideration is the following.

It was mentioned earlier that most overpressures occur before 5 percent of the total projectile travel has occurred. The fraction of the charge burned that corresponds to this is about 20 percent. This varies somewhat from charge to charge but it is fairly accurate for most high performance guns. Therefore, in this analysis the time required to burn normal grains within the MCB to 20 percent fraction burned once proper ignition was established was 5.2 ms. The fraction burned after this same length of time was marked for each closed bomb firing of damaged JA2 grains. Table 2 shows the values that were found. As expected, the more damaged the grains were, the greater the amount of propellant that was burned within that time. The fraction burned corresponding to that time was used as the upper limit on the integral of the Area Ratio Deviation vs Fraction Burned curve instead of using the entire deviation curve. This, then, should enable better comparison of the effective mass generation of damaged and undamaged propellants. The results are shown in Figure 14. Figure 14a

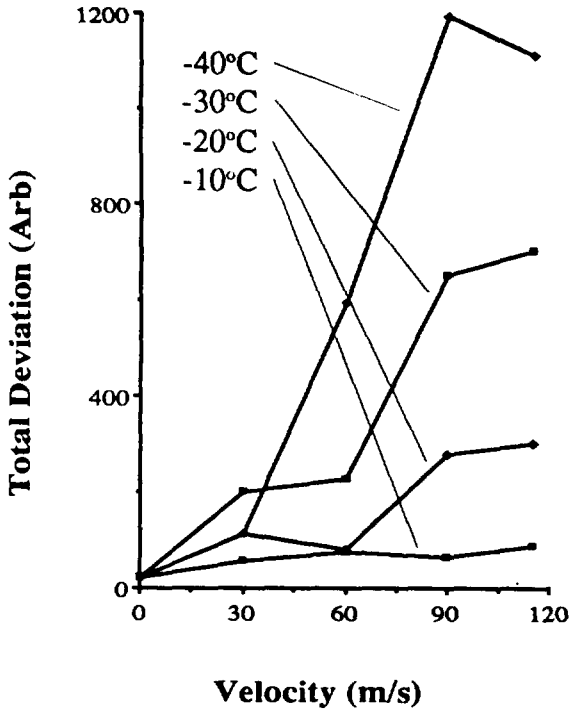

Figure 14a. Total Deviation vs Velocity for JA2

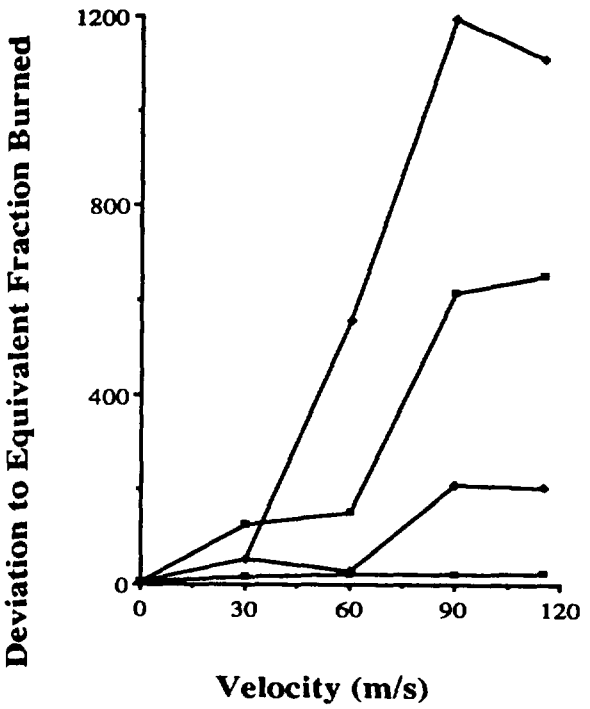

Figure 14b. Deviation at Equivalent Fraction Burned Calculated from the Same Data as Used in Figure 14a

Figure 14. Comparison of TD and a Weighted TD to Compensate for Equivalent Mass Burned

shows the TD values using the entire deviation curves, while Figure 14b was calculated only using the time equivalent fraction burned as described above. There is no marked differences between the information in either set of curves. The relative magnitude of the differences in the curves is changed, but the order of fracture damage ranking remains the same. Most of the attempts to modify this information to extract greater information have had similar results.

C. DWMPT Post-Failure Parameter

The TD information, as mentioned, was gathered with considerable effort. The usefulness of a fracture susceptibility parameter that is eventually developed will depend to a large degree on how easily the information required can be generated. This is true from the standpoint of the availability of equipment, and the difficulty of the experimental procedure and analysis. It is with these thoughts in mind that other considerations are under investigation for a parameter that can be determined utilizing conventional equipment and standard testing procedures. These investigations involve post-failure measurements that will reveal the the propensity of the material to fracture failure.

One measurement under consideration is called the Failure Modulus, E_f, which is defined in the usual manner except that post failure information is used. The relationship is defined as

$$E_f = - \frac{d\sigma_f}{d\varepsilon_f} , \qquad (3)$$

TABLE 2. PERCENT OF GGIT DAMAGED PROPELLANT BURNED IN THE MCB AFTER 5.2 ms

Temperature = T, Fraction Burned at Impact Velocity X m/s = FB(X)

T °C	FB(30) %	FB (60) %	FB(90) %	FB (115) %
-10	23	19	24	23
-20	28	23	42	37
-30	30	34	71	75
-40	26	65	96	91

where σ_f and ε_f are the post-failure stress and strain, respectively. If plastic flow is the main failure mode, as in Figures 1a and 3a, E_f will have a low value. As failure becomes more brittle, as is the case as the temperature is lowered in Figure 1, the value of E_f increases. Under extremely brittle conditions very high values for E_f should be measured. What E_f measures is the ability of the material to support a load after failure has occurred. This will relate to the amount of fracture that occurs subsequent to failure, which reduces the area able to support the applied load. The parameter derivation is shown schematically in Figure 15.

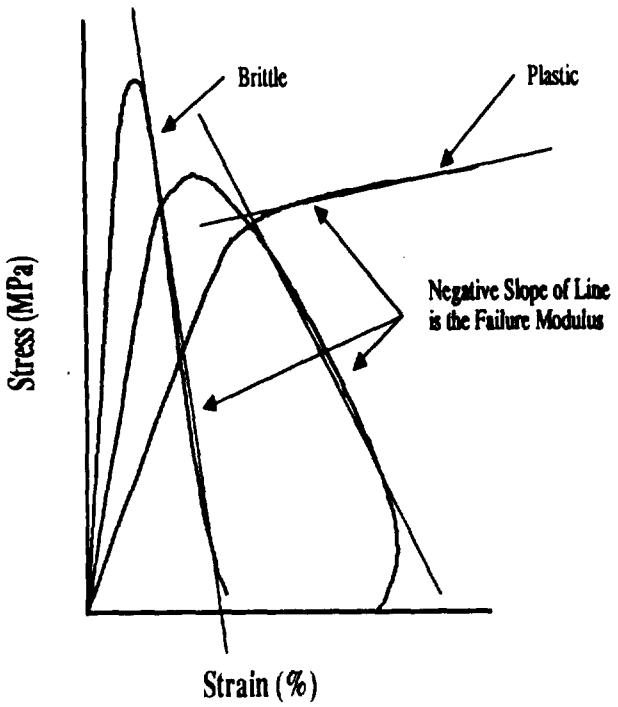

Figure 15. Schematic Diagram of Stress vs Strain Illustrating the Failure Modulus Concept

Figure 16a shows the Modulus and Failure Modulus for M30 as a function of temperature from DWMPT. The low values at the higher temperatures show good ability to support a load after failure. The higher values at lower temperatures indicate more brittle behavior due to the more rapid fall in ability to support stress as deformation increases. The Failure Modulus needs some further modification to be able to compare situations involving materials of different moduli. To explain, consider the following. If two materials had the same brittleness, suffered loss of strength due to identical fracture, and one had a lower modulus than the other, then the failure modulus for the higher modulus material would be greater. Since the amount of generated fracture is the quantity to be isolated, normalizing the failure modulus is required. To normalize the Failure Modulus the ratio of the Failure Modulus to the Modulus (the curves shown

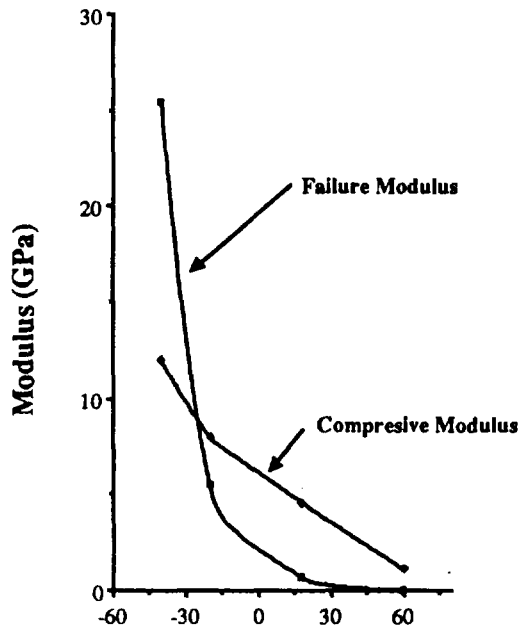

Figure 16a. Compressive and Failure Modulus vs Temperature

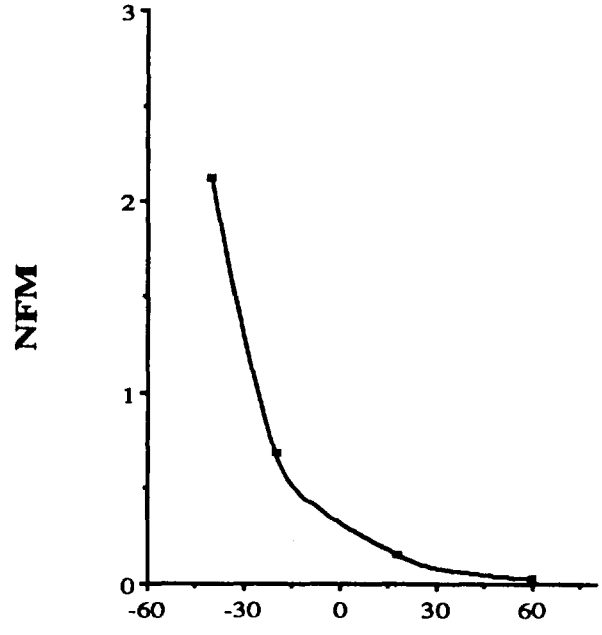

Figure 16b. Normalized Failure Modulus vs Temperature

Figure 16. Comparison of Compressive, Failure, and Normalized Failure Modulus from DWMPT Data for M30 Propellant

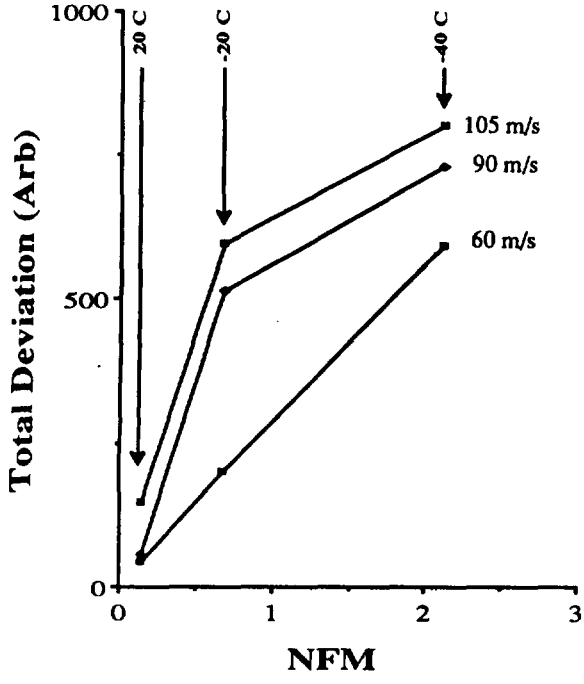

Figure 17. Total Deviation vs NFM for M30

in Figure 16a) is calculated. The result is the Normalized Failure Modulus (NFM) which for M30 is shown in Figure 16b. This parameter can be used to correlate this test with other tests which measure fracture susceptibility more directly. Such a correlation is shown in Figure 17, where the TD for M30 is plotted against the NFM. In these curves, the points corresponding to the same temperature are plotted using their associated TD and NFM values. Each curve corresponds to a separate GGIT impact velocity, as indicated. This procedure offers a method to obtain fracture information from propellant types from a relatively simple mechanical properties test procedure.

Another test procedure under consideration, which is quite similar to the

above, involves damaging a specimen under specific conditions and then performing subsequent mechanical properties measurements on the damaged specimen. The ratio of the "Damaged Modulus" to the Modulus could be correlated with GGIT fracture damage parameters. Changes in the mechanical response of the damaged specimens could indicate the amount of damage suffered in a way similar to the previously outlined procedure for the NFM.

The development of both of these procedures will begin as soon as the high rate servohydraulic testing facility (SHT) is installed at BRL. This tester is capable of program controlled compressive/tensile testing at strain rates up to 1000/s. The device will also eliminate some post-failure measurement problems encountered with the DWMPT. The impact of the weight cage and the ram in the DWMPT causes the load to be applied to the specimen in pulses. The SHT will apply post failure stresses in a continuous fashion which should facilitate failure modulus measurements. The SHT will also be able to damage specimens to a predetermined stress/strain and otherwise enhance the measurement capabilities of BRL's propellant mechanical properties facility.

VII. FRACTURE DAMAGE MODEL FOR AN INTERIOR BALLISTIC CODE

Efforts are under way to include the fracture generated surface area described in this report into the one dimensional hydrodynamic interior ballistic code XNOVAKTC[8,9]. A method that could be used to evaluate any mechanical damage is outlined in Figure 18. Damage can come from three sources: i. perforation rupture, ii. direct grain impact, and iii. intergranular stress.

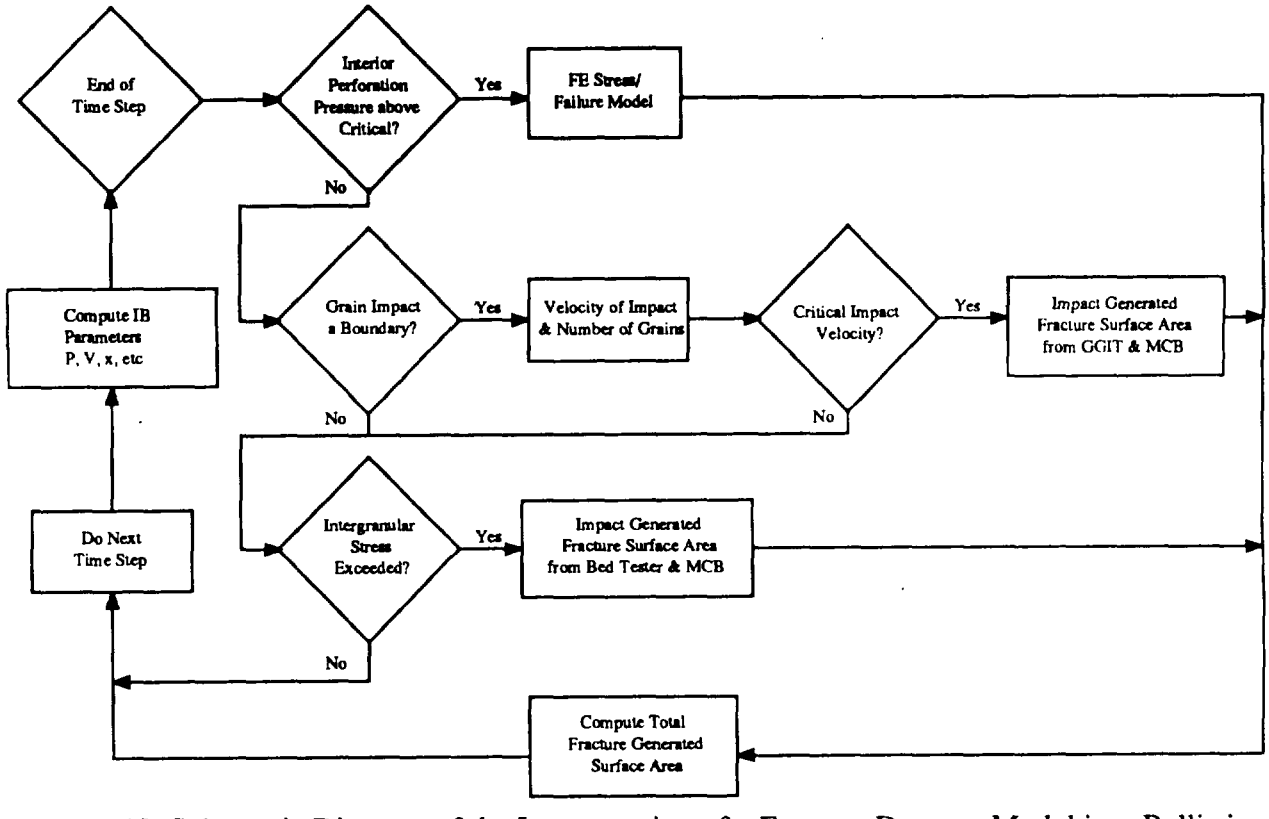

Figure 18. Schematic Diagram of the Incorporation of a Fracture Damage Model into Ballistic Codes

i. Excessive perforation pressure arises when mass generation within the perforation exceeds the mass flow out of the perforation ends. When the a critical pressure is reached, based on failure stresses and finite element grain models, the perforation ruptures and new surface area is generated.

ii. Since the propellant velocity can be calculated within the code any impact condition can be calculated for a grain on the propellant bed boundary. The resulting fracture damage can be evaluated from Area Ratio vs Fraction Burned profiles.

iii. Measurements done previously with a high rate propellant bed tester [10,11] indicate that intergranular stresses produce fracture generated surface area in amounts comparable to direct grain impact. The damage generated due to specific levels of intergranular stress will be measured in a fashion similar to that of the single impact grain damage.

Additional burning surface area from each of these sources can be included in mass generation equations. Since this code is hydrodynamic, as opposed to thermodynamic, it can predict the generation of pressure waves and local areas of increased pressurization. Both of these phenomena play an important role in high pressure events. These dynamics will help predictions to become more real, and the interactions between the mechanical response and the pressurization will be better understood.

VIII. CONCLUSIONS

The ability to address the question of fracture susceptibility of gun propellants and how the resulting fracture affects propellant combustion are beginning to be addressed. The mechanical property measurements and fracture generated surface area profiles for impact damaged grains have been established over a wide range of conditions that approach those of the early interior ballistic cycle for M30 and JA2 propellant. Methods are being developed to establish correlations between the fracture generated surface area and mechanical properties parameters. One of these parameters, the Normalized Failure Modulus correlates well with the fracture generated surface area. The NFM is easily measured and may serve as a quick guide for evaluating the fracture susceptibility of a particular propellant once a damage profile for a class of propellants has been established, i.e. single, double, or triple base; nitramine composite; thermoplastic elastomer; etc. The NFM is measured after failure has occurred and, therefore, deviates from traditional mechanical properties measurements which generally characterize the pre-failure response.

The XNOVAKTC code is a one dimensional, two phase, hydrodynamic code that can predict propellant velocities and probe the effects of local pressurization and propellant fracture location. As indicated, the amount of grain fracture that will be used in the code at various velocities and temperatures will be based on mechanical properties information presently in hand.

Future research will continue to focus on establishing the parameters and test methods that permit the role of propellant fracture to be understood and predicted within guns. The addition of the high rate servohydraulic tester to the BRL mechanical properties test facility will significantly increase the ability to characterize propellant mechanical response and isolate complex propellant variables.

IX. ACKNOWLEDGMENTS

The author would like to specially thank Mike Leadore who gathered a significant portion of these data with great care and diligence. Also, thanks are due to F. W. Robbins and A. A. Juhasz, who provided insight into interior ballistic and closed bomb information related to these studies.

REFERENCES

1. F. W. Robbins, Private Communication, BRL.

2. M. Costantino and D. Ornellas, "The High Pressure Failure Curve for JA2," 1987 JANNAF Structures & Mechanical Behavior Subcommittee Meeting, Volume I, CPIA Publication 463, pp 73-80, March 1987.

3. R. J. Lieb, and J. J. Rocchio, "Standardization of a Drop Weight Mechanical Properties Tester for Gun Propellants," Technical Report ARBRL-TR-02516, USA ARRADCOM Ballistic Research Laboratory, Aberdeen Proving Ground, Maryland, July 1983.

4. R. J. Lieb, and J. J. Rocchio, "A Gas Gun Impact Tester for Solid Gun Propellants," Memorandum Report BRL-MR-3399, USA Ballistic Research Laboratory, Aberdeen Proving Ground, Maryland, October 1984.

5. R. J. Lieb, D. Devynck, and J. J. Rocchio, "The Evaluation of High Rate Fracture Damage of Gun Propellant Grains," 1983 JANNAF Structure and Mechanical Behavior Subcommittee Meeting, CPIA Publication 388, pp 177-185, November 1983.

6. R. J. Lieb, and J. J. Rocchio, "Velocity-Temperature Fracture Damage Profile of Gun Propellant Grains," 1984 JANNAF CMCS/S&MBS Joint Subcommittee Meeting, Volume I, CPIA Publication 418, pp 303-312, November 1984.

7. C.F. Davis and D. Smith, "The Shotgun Test - A Tool for Evaluating Solid Propellants," Contractor Report, DAAD05-80-M-8776, Hercules Incorporated, 1981.

8. P. S. Gough, "The NOVA Code: A User's Manual," Indian Head Contract Report IHCR80-8, 1980.

9. P. S. Gough, Contractor Report, DAAK11-85-D-0002, in preparation.

10. R. J. Lieb, "Surface Area Analysis of Grain-Grain Impact of Gun Propellants,"1986 JANNAF Structures & Mechanical Behavior Subcommittee Meeting, CPIA Publication 449, pp 109-116, April 1986.

11. R. J. Lieb, "High Rate Intrinsic Bed Response of Gun Propellant," 1987 JANNAF Structures & Mechanical Behavior Subcommittee Meeting, Volume I, CPIA Publication 463, pp 51-62, March 1987.

DISTRIBUTION LIST

No. Of Copies	Organization
12	Administrator Defense Technical Info Center ATTN: DTIC-DDA Cameron Station Alexandria, VA 22304-6145
1	Commander USA Concepts Analysis Agency ATTN: D. Hardison 8120 Woodmont Avenue Bethesda, MD 20014-2797
1	HQDA/DAMA-ZA Washington, DC 20310-2500
1	HQDA, SARDA Washington, DC 20310-2500
1	Commander US Army War College ATTN: Library-FF229 Carlisle Barracks, PA 17013
1	US Army Ballistic Missile Defense Systems Command Advanced Technology Center P.O. Box 1500 Huntsville, AL 35807-3801
1	Commander US Army Materiel Command ATTN: AMCDRA-ST 5001 Eisenhower Avenue Alexandria, VA 22333-5001
1	Commander US Army Materiel Command ATTN: AMCDE-DW 5001 Eisenhower Avenue Alexandria, VA 22333-5001
5	Project Manager Cannon Artillery Weapons System, ARDEC, AMCCOM ATTN: AMCPM-CW, F. Menke AMCPM-CWW AMCPM-CWS M. Fisette AMCPM-CWA R. DeKleine H. Hassmann Dover, NJ 07801-5001
2	Project Manager Munitions Production Base Modernization and Expansion ATTN: AMCPM-PBM, A. Siklosi AMCPM-PBM-E, L. Laibson Dover, NJ 07801-5001
3	Project Manager Tank Main Armament Systems ATTN: AMCPM-TMA, K. Russell AMCPM-TMA-105 AMCPM-TMA-120 Dover, NJ 07801-5001
1	Commander US Army Watervliet Arsenal ATTN: SARWV-RD, R. Thierry Watervliet, NY 12189-5001

No. Of Copies	Organization
1	Chairman DOD Explosives Safety Board Room 856-C Hoffman Bldg. 1 2461 Eisenhower Avenue Alexandria, VA 22331-9999
1	Commander US Army Material Command ATTN: AMCPM-GCM-WF 5001 Eisenhower Avenue Alexandria, VA 22333-5001
1	Commander Armament R&D Center US Army AMCCOM ATTN: SMCAR-TDC Picatinny Arsenal, NJ 07806-5000
4	Commander US Army Armament Munitions and Chemical Command ATTN: SMCAR-ESP-L Rock Island, IL 61299-7300
1	Commander US Army Aviation Research and Development Command ATTN: AMSAV-E 4300 Goodfellow Blvd. St. Louis, MO 63120-1702
1	Commander Armament R&D Center US Army AMCCOM ATTN: SMCAR-TSS Picatinny Arsenal, NJ 07806-5000
20	Commander US Army ARDEC ATTN: SMCAR-TSS SMCAR-TDC SMCAR-LC LTC N. Baron SMCAR-LCA A. Beardell D. Downs S. Einstein S. Westley S. Bernstein C. Roller J. Rutkowski SMCAR-LCB-I D. Spring SMCAR-LCE SMCAR-LCM-E S. Kaplowitz SMCAR-LCS SMCAR-LCU-CT E. Barrieres R. Davitt SMCAR-LCU-CV C. Mandala SMCAR-LCW-A M. Salsbury SMCAR-SCA L. Stiefel B. Brodman Picatinny Arsenal, NJ 07806-5001
1	Director Benet Weapons Laboratory Armament R&D Center US Army AMCCOM ATTN: SMCAR-LCB-TL Watervliet, NY 12189-5001
1	Commander US Army TSARCOM 4300 Goodfellow Blvd. St. Louis, MO 63120-1702

No. Of Copies	Organization
1	HQDA DAMA-ART-M Washington, DC 20310-2500
1	Director US Army Air Mobility Research and Development Laboratory Ames Research Center Moffett Field, CA 94035-1099
1	Commander US Army Harry Diamond Lab ATTN: DELHD-TA-L 2800 Powder Mill Road Adelphi, MD 20783-1145
1	Commander US Army Missile and Space Intelligence Center ATTN: AIAMS-YDL Redstone Arsenal, AL 35898-5500
1	Commander US Army Missle Command Research, Development, and Engineering Center ATTN: AMSMI-RD Redstone Arsenal, AL 35898-5500
1	Commandant US Army Aviation School ATTN: Aviation Agency Fort Rucker, AL 36360
1	Commander US Army Tank Automotive Command ATTN: AMSTA-TSL Warren, MI 48397-5000
1	Commander US Army Tank Automotive Command ATTN: AMSTA-CG Warren, MI 48397-5000

No. Of Copies	Organization
1	Commander US Army Communications Electronics Command ATTN: AMSEL-ED Fort Monmouth, NJ 07703-5301
1	Commander ERADCOM Technical Library ATTN: DELSD-L (Report Section) Fort Monmouth, NJ 07703-5301
1	Commander US Army Missile Command ATTN: AMSMI-CM Redstone Arsenal, AL 35898-5249
1	President US Army Armor & Engineer Board ATTN: ATZK-AD-S Fort Knox, KY 40121-5200
1	Project Manager M-60 Tank Development ATTN: AMCPM-M60TD Warren, MI 48092-2498
1	Director TRADOC Analysis Command - White Sands Missile Range ATTN: ATAA-SL White Sands Missle Range, NM 88002-5502
1	Commander TRADOC Analysis Command ATTN: ATRC-MA/MAJ Williams Fort Monroe, VA 23651-5143
2	Commander US Army Materials and Mechanics Research Center ATTN: AMXMR-ATL Tech Library Watertown, MA 02172

No. Of Copies	Organization
1	Project Manager Improved TOW Vehicle ATTN: AMCPM-ITV US Army Tank Automotive Command Warren, MI 48397-5000
2	Program Manager M1 Abrams Tank System ATTN: AMCPM-GMC-SA, T. Dean Warren, MI 48092-2498
1	Project Manager Fighting Vehicle Systems ATTN: AMCPM-FVS Warren, MI 48092-2498
1	Commandant US Army Infantry School ATTN: ATSH-CD-CSO-OR Fort Benning, GA 31905
1	Office of Naval Research ATTN: Code 473, R.S. Miller 800 N. Quincy Street Arlington, VA 22217-9999
1	Commandant US Army Command and General Staff College Fort Leavenworth, KS 66027
1	Commandant US Army Special Warfare School ATTN: Rev & Tng Lit Div Fort Bragg, NC 28307
3	Commander Radford Army Ammunition Plant ATTN: SMCRA-QA/HI LIB Radford, VA 24141-0298
1	Commander US Army Foreign Science & Technology Center ATTN: AMXST-MC-3 220 Seventh Street, NE Charlottesville, VA 22901-5396
1	Commander US Army Research Office ATTN: Tech Library P.O. Box 12211 Research Triangle Park, NC 27709-2211
1	Commander US Army Belvoir Research & Development Center ATTN: STRBE-WC Fort Belvoir, VA 22060-5606
1	Commander US Army Logistics Mgmt Ctr Defense Logistics Studies Fort Lee, VA 23801
1	President US Army Artillery Board Ft. Sill, OK 73503-5600
3	Commandant US Army Armor School ATTN: ATZK-CD-MS M. Falkovitch Armor Agency Fort Knox, KY 40121-5215
2	Commander Naval Sea Systems Command ATTN: SEA 62R SEA 64 Washington, DC 20362-5101
1	Commander Naval Air Systems Command ATTN: AIR-954-Tech Lib Washington, DC 20361-9300
1	Assistant Secretary of the Navy (R, E, and S) ATTN: R. Reichenbach Room 5E787 Pentagon Bldg. Washington, DC 20350

No. Of Copies	Organization
1	Naval Research Lab Tech Library Washington, DC 20375
5	Commander Naval Surface Weapons Center ATTN: Code G33, J.L. East W. Burrell J. Johndrow Code G23, D. McClure Code DX-21 Tech Lib Dahlgren, VA 22448-5000
2	Commander US Naval Surface Weapons Center ATTN: J.P. Consaga C. Gotzmer Indian Head, MD 20640-5000
4	Commander Naval Surface Weapons Center ATTN: S. Jacobs/Code 240 Code 730 K. Kim/Code R-13 R. Bernecker Silver Springs, MD 20903-5000
2	Commanding Officer Naval Underwater Systems Center Energy Conversion Dept. ATTN: Code 5B331, R.S. Lazar Tech Library Newport, RI 02840
4	Commander Naval Weapons Center ATTN: Code 388, R.L. Derr C.F. Price T. Boggs Info. Sci. Div. China Lake, CA 93555-6001
2	Superintendent Naval Postgraduate School Department of Mechanical Engineering Monterey, CA 93943-5100
2	Commandant US Army Field Artillery Center & School ATTN: ATSF-CO-MW, B. Willis Ft. Sill, OK 73503-5600
1	Commander US Army Development and Employment Agency ATTN: MODE-TED-SAB Fort Lewis, WA 98433-5099
6	Commander Naval Ordnance Station ATTN: P.L. Stang J. Birkett L. Torreyson T.C. Smith D. Brooks Tech Library Indian Head, MD 20640-5000
1	AFSC/SDOA Andrews AFB, MD 20334
1	AFRPL/DY, Stop 24 ATTN: J. Levine/DYCR R. Corley/DYC D. Williams/DYCC Edwards AFB, CA 93523-5000
1	AFRPL/TSTL (Tech Library) Stop 24 Edwards AFB, CA 93523-5000
1	AFATL/DLYV Eglin AFB, FL 32542-5000
1	AFATL/DLXP Eglin AFB, FL 32542-5000
1	AFATL/DLJE Eglin AFB, FL 32542-5000
1	AFATL/DLODL ATTN: Tech Library Eglin AFB, FL 32542-5000

No. Of Copies	Organization
1	AFWL/SUL Kirtland AFB, NM 87117
1	NASA/Lyndon B. Johnson Space Center ATTN: NHS-22, Library Section Houston, TX 77054
1	AFELM, The Rand Corporation ATTN: Library D (Required or 1700 Main Street Classified Santa Monica, CA only) 90401-3297
1	General Applied Sciences Lab ATTN: J. Erdos Merrick & Stewart Avenues Westbury Long Island, NY 11590
1	AAI Corporation ATTN: J. Hebert J. Frankle P.O. Box 6767 Baltimore, MD 21204
	Aerojet Ordnance Company ATTN: D. Thatcher 2521 Michelle Drive Tustin, CA 92680-7014
1	Aerojet Solid Propulsion Co. ATTN: P. Micheli Sacramento, CA 95813
1	Atlantic Research Corporation ATTN: M.K. King 5390 Cheorokee Avenue Alexandria, VA 22312-2302

No. Of Copies	Organization
1	Program Manager AFOSR Directorate of Aerospace Sciences ATTN: L.H. Caveny Bolling AFB, DC 20332-0001
2	Calspan Corporation ATTN: C. Morphy P.O. Box 400 Buffalo, NY 14225-0400
10	Central Intelligence Agency Office of Central Reference Dissemination Branch Room GE-47 HQS Washington, DC 20505
1	General Electric Company Armament Systems Dept. ATTN: M.J. Bulman, Room 1311 128 Lakeside Avenue Burlington, VT 05401-4985
1	IITRI ATTN: M.J. Klein 10 W. 35th Street Chicago, IL 60616-3799
1	Hercules, Inc. Allegheny Ballistics Laboratory ATTN: R.B. Miller P.O. Box 210 Cumberland, MD 21501-0210
1	Hercules, Inc. Bacchus Works ATTN: K.P. McCarty P.O. Box 98 Magna, UT 84044-0098
1	Hercules, Inc. Radford Army Ammunition Plant ATTN: J. Pierce Radford, VA 24141-0299
1	AVCO Everett Rsch Lab ATTN: D. Stickler 2385 Revere Beach Parkway Everett, MA 02149-5936

No. Of Copies	Organization
1	Honeywell, Inc - MN64 2200 Defense Systems Division ATTN: C. Hargreaves 6110 Blue Circle Drive Minnetonka, MN 55436
1	Lawrence Livermore National Laboratory ATTN: L-355, A. Buckingham M. Finger P.O. Box 808 Livermore, CA 94550-0622
1	Lawrence Livermore National Laboratory ATTN: L-324 M. Constantino P.O. Box 808 Livermore, CA 94550-0622
1	Olin Corporation Badger Army Ammunition Plant ATTN: R.J. Thiede Baraboo, WI 53913
1	Olin Corporation Smokeless Powder Operations ATTN: D.C. Mann P.O. Box 222 St. Marks, FL 32355-0222
1	Paul Gough Associates, Inc. ATTN: P.S. Gough P.O. Box 1614, 1048 South St. Portsmouth, NH 03801-1614
1	Physics International Company ATTN: Library H. Wayne Wampler 2700 Merced Street San Leandro, CA 94577-5602
2	United Technologies Chemical Systems Division ATTN: R. Brown Tech Library P.O. Box 358 Sunnyvale, CA 94086-9998
1	Princeton Combustion Research Lab., Inc. ATTN: M. Summerfield 475 US Highway One Monmouth Junction, NJ 08852-9650
2	Rockwell International Rocketdyne Division ATTN: BA08 J.E. Flanagan J. Gray 6633 Canoga Avenue Canoga Park, CA 91303-2703
1	Science Applications, Inc. ATTN: R.B. Edelman 23146 Cumorah Crest Drive Woodland Hills, CA 91364-3710
3	Thiokol Corporation Huntsville Division ATTN: D. FLanigan R. Glick Tech Library Huntsville, AL 35807
1	Scientific Research Assoc., Inc. ATTN: H. McDonald P.O. Box 498 Glastonbury, CT 06033-0498
1	Veritay Technology, Inc. ATTN: E. Fisher 4845 Millersport Hwy. P.O. Box 305 East Amherst, NY 14051-0305
2	Thiokol Corporation Elkton Division ATTN: R. Biddle Tech Lib. P.O. Box 241 Elkton, MD 21921-0241
1	University of Massachusetts Dept. of Mechanical Engineering ATTN: K. Jakus Amherst, MA 01002-0014

No. Of Copies	Organization
1	Universal Propulsion Company ATTN: H.J. McSpadden Black Canyon Stage 1 Box 1140 Phoenix, AZ 85029
1	Battelle Memorial Institute ATTN: Tech Library 505 King Avenue Columbus, OH 43201-2693
1	Brigham Young University Dept of Chemical Engineering ATTN: M. Beckstead Provo, UT 84601
1	California Institute of Tech 204 Karman Lab Main Stop 301-46 ATTN: F.E.C. Culick 1201 E. California Street Pasadena, CA 91109
1	California Institute of Tech Jet Propulsion Laboratory ATTN: L.D. Strand 4800 Oak Grove Drive Pasadena, CA 91109-8099
1	University of Illinois Dept of Mech/Indust Engr ATTN: H. Krier 144 MEB; 1206 N. Green St. Urbana, IL 61801-2978
1	University of Minnesota Dept of Mechanical Engineering ATTN: E. Fletcher Minneapolis, MN 55414-3368
1	Case Western Reserve University Division of Aerospace Sciences ATTN: J. Tien Cleveland, OH 44135
3	Georgia Institute of Tech School of Aerospace Eng. ATTN: B.T. Zinn E. Price W.C. Strahle Atlanta, GA 30332
1	Institute of Gas Technology ATTN: D. Gidaspow 3424 S. State Street Chicago, IL 60616-3896
1	Johns Hopkins University Applied Physics Laboratory Chemical Propulsion Information Agency ATTN: T. Christian Johns Hopkins Road Laurel, MD 20707-0690
1	Massachusetts Institute of Technology Dept of Mechanical Engineering ATTN: T. Toong 77 Massachusetts Ave Cambridge, MA 02139-4307
1	G.M. Faeth Pennsylvania State University Applied Research Laboratory University Park, PA 16802-7501

No. Of Copies	Organization
1	University of Southern California Mechanical Engineering Dept. ATTN: OHE200, M. Gerstein Los Angeles, CA 90089-5199
2	University of Utah Dept of Chemical Engineering ATTN: A. Baer G. Flandro Salt Lake City, UT 84112-1194
1	Washington State University Dept of Mechanical Engineering ATTN: C.T. Crowe Pullman, WA 99163-5201
1	Rensselaer Polytechnica Inst. Department of Mathematics Troy, NY 12181
1	Rutgers University Dept of Mechanical and Aerospace Engineering ATTN: S. Temkin University Heights Campus New Brunswick, NJ 08903
1	Pennsylvania State University Dept of Mech. Engineering ATTN: K. Kuo University Park, PA 16802-7501
1	Purdue University School of Mechanical Engineering ATTN: J.R. Osborn TSPC Chaffee Hall West Lafayette, IN 47907-1199
1	SRI International Propulsion Sciences Division ATTN: Tech Library 333 Ravenswood Ave Menlo Park, CA 94025-3493
1	Stevens Institute of Technology Davidson Laboratory ATTN: R. McAlevy, III Castle Point Station Hoboken, NJ 07030-5907

<u>Aberdeen Proving Ground</u>

Dir, USAMSAA
ATTN: AMXSY-D
AMXSY-MP, H. Cohen
Cdr, USATECOM
ATTN: AMSTE-TO-F
AMSTE-CM-F, L. Nealley
Cdr, CSTA
ATTN: STECS-AS-H, R. Hendricksen
Cdr, CRDEC, AMCCOM
ATTN: SMCCR-RSP-A
SMCCR-MU
SMCCR-MSI